Electronic and magnetic features of twisted spin-density-wave states in the two-dimensional Hubbard model

Sajeev John, Puru Voruganti, and William Goff
Department of Physics, University of Toronto, Toronto, Ontario, Canada M5S 1A7
(Received 5 November 1990)

Using a path-integral formalism and decomposing the Hubbard interaction into charge and spin order parameters, we develop a $1/S$ loop expansion of the two-dimensional Hubbard model. At the saddle-point level, we present a detailed study of the energetics of twisted antiferromagnetic order. Doping the antiferromagnetic state leads to a rich mean-field phase diagram at zero temperature, which includes spiral phases, a column phase, and ferromagnetism. The on-site magnetization, the density of states, the plasma frequency, and the quasiparticle weights are evaluated for the twisted spin-density-wave (SDW) states as a function of doping and U/t. Doping-induced frustration remarkably leads to a closure of the Mott-Hubbard band gap for any U/t. At one-loop order, we delineate the collective spin and charge fluctuations of the mean-field SDW state. The action for the two transverse spin modes at half-filling maps to a nonlinear σ model, which tends to disorder upon doping. Twisted magnetic ground states exhibit a third Goldstone mode due to the complete breaking of rotational invariance. For the commensurate SDW, the charge fluctuations couple only to longitudinal spin fluctuations, whereas, for the incommensurate metallic SDW states, the charge modes are coupled nontrivially to the massless spin waves. This suggests a metallic state quite unlike traditional Fermi liquids.

I. INTRODUCTION

The electronic and magnetic properties of Mott insulators[1] present a long-standing fundamental problem in solid-state physics. These systems have received renewed interest because of their relevance to the recently discovered[2] high-temperature oxide superconductors.[3] The fundamental issue is the precise description of a low-dimensional strongly correlated electron system as in the two-dimensional (2D) Hubbard model[4] where the application of standard many-body methods is highly problematic. The two-dimensional character of the layered perovskite superconductors suggests that expansions about standard spin-density-wave (SDW) mean fields would be inefficient due to strong fluctuation effects. This has led many authors to use as their starting point exact solutions of one- and two-dimensional model Hamiltonians where no long-range magnetic order is found at finite temperature. In this approach, the observed antiferromagnetic order for the undoped Mott insulator would later be accounted for by adding weak interlayer couplings to an exact solution of a strictly two-dimensional model. The advantage of this approach is that it can incorporate from the outset one of the salient features of the perovskite superconductors, namely the non-Fermi-liquid behavior observed in the normal metallic phase at finite doping. The disadvantage of this approach is that the two-dimensional model is itself poorly understood. Even in the preliminary phase of the calculation, some other mean-field approximation must be introduced and its fluctuation corrections established. In this paper, we adopt the view that weak interlayer couplings may, in fact, stabilize SDW mean-field approximations to the 2D Hubbard model and that it is meaningful to consider fluctuations about such a broken-symmetry state even at finite temperature. These fluctuations take two forms. The first are small-amplitude charge and spin-wave fluctuations whereas the second class of corrections involve large-amplitude distortions of the magnetic mean field such as domain walls, solitons, and instantons. We find that a possible source of non-Fermi-liquid behavior emerges from even small-amplitude fluctuations when there is a twist in the underlying mean-field magnetic order. Whereas in the undoped antiferromagnet, the charge fluctuation mode has a mass given by the Mott-Hubbard (MH) interband gap; in the doped system, the fluctuation spectrum exhibits massless intraband excitations across the Fermi surface. In the presence of the twist, however, the off-diagonal spin-charge response for the metallic state no longer vanishes and is already manifest at the mean-field level by the gradual variation of the pitch with doping. This unique coupling of collective charge fluctuations to massless spin waves realizes an intriguing variation of the usual conductivity dominated by low-energy particle-hole excitations alone. In addition, the intrinsic two-dimensional nature of the magnetic ordering in twisted SDW ground states leads to an additional massless spin-wave mode in contrast to only two Goldstone modes for antiferromagnetism. Moreover, the macroscopic shift of the ground-state wave function parametrized by the pitch through doping implies that the spiral metal is quite unlike traditional Fermi liquids.

Theoretical approaches based on SDW mean-field solutions predict that, at least for small doping and sufficiently large U/t, incommensurate magnetic states[5] should exist while other works based on exact solutions

of lower-dimensional models stress the importance of resonating valence bond,[6] flux,[7] chiral,[8] or topological ordered phases[9] in the Hubbard model or its derivative, the t-J model. μSR experiments indicate that the on-site magnetization is reduced by up to 50% prior to the onset of superconductivity and neutron scattering reveals short-range magnetic order rather than a prominent Bragg peak at finite doping δ with a correlation length $\xi \sim \delta^{-1/2}$ and spin-wave velocities considerably lowered upon doping. Short-range correlations are also evident from NMR data. Dynamic short-ranged antiferromagnetic correlations are evident in disordered ground states of low-dimensional models, whereas incommensurate SDW states exhibit static long-range order with a reduced on-site magnetization. However, these latter states may also be disordered by fluctuation effects. The fact that spiral states can twist either clockwise or counterclockwise in a given direction leads to new degeneracies of the ground state. If parity remained a good symmetry, then the domains that arise between these degenerate solutions could also naturally account for the short-range magnetism. On the electronic side, the anomalous properties of the charge carriers in the Raman data, dc conductivity may provide a stronger test of theory. A full explanation of these facts may lie not only in spin-charge separation for the carriers that naturally appears in the one-dimensional Hubbard model but also in the influence of the upper Mott-Hubbard band.[10] The upper Hubbard band describes the doubly occupied sites which, for positive U, are the antibound states. Their effect on the normal-state electronic properties of the quasiparticles depends strongly on their proximity to the Fermi surface. Interestingly, even for large U/t, the variation of the pitch of the spiral states and the depressed local magnetic moment conspire to not only close the Mott-Hubbard band gap but also bring these antibound states arbitrarily close to the Fermi level for moderate doping. Although neither the crossing nor the proximity have a significant effect on the quasiparticle weights at the mean-field level, their contribution as virtual states in standard response functions will be nontrivial.

An additional difficulty in the many-body theory of the strongly correlated Hubbard model is the absence of any convergence parameter for fluctuation effects even at zero temperature. Convergence of an expansion about a SDW state can nevertheless be provided by extending the spin degeneracy of electrons to N_f flavors. For SDW mean fields, we show that this trick facilitates a perturbation expansion in $1/N_f$ for the correlation functions at any U/t for the Hubbard model, which, in turn, allows us to make contact with many experimentally observed features of the quasi-two-dimensional perovskite superconductors.

In Sec. II, we develop the path-integral formulation and recast the Hubbard interaction into charge and spin order parameters via the usual Hubbard-Stratonovich transformations. By expanding about a SDW saddle point and integrating over the fermions, we obtain an effective Landau-Ginzburg functional for the order-parameter fields perturbative in $1/S$. In Sec. III, the saddle-point solutions are evaluated at filling $0.01 \leq \delta \leq 0.6$ and $2 < U/t < 15$. Having obtained the magnetic phase diagram, we compute the spectral density, the quasiparticle weights, the plasma frequency, and the band-closure line. From the energetics of the mean-field states, the phase separated regions are identified. In Sec. IV, we consider the one-loop level to establish the stability of the SDW saddle point and find the quadratic Landau-Ginzburg action for the broken-symmetry mean-field states. At half-filling, the nonlinear σ model is thus directly derived from the Hubbard model and we compute the variation of the σ-model coupling constant with doping confirming that doping disorders the antiferromagnet. For the incommensurate SDW, we delineate three massless spin-wave branches and their coupling to the spin-amplitude and charge-fluctuation modes. Lastly, in Sec. V, we provide a summary and connections of this work to experimental signatures.

II. 1/S EXPANSION

The model appropriate to the strongly correlated problem for the layered perovskites will be taken to be the one-band Hubbard Hamiltonian[3] with on-site repulsion U an order of magnitude larger than the bandwidth parameter t:

$$H = -t \sum_{ij} c_{i\alpha}^{\dagger} c_{i\alpha} + U \sum_{i} n_{i\uparrow} n_{i\downarrow} \, . \tag{1}$$

Here, the sum is performed over all nearest neighbors and the spin index $\alpha = 1,2$ for up and down spins, respectively. The partition function

$$\mathrm{Tr}[\exp -\beta(H - \mu_0 N)]$$

with μ_0 being the chemical potential, $k_B T = 1/\beta$, and $N = \sum_i c_{i\alpha}^{\dagger} c_{i\alpha}$ can be expressed as an imaginary-time coherent-state path integral:

$$\begin{aligned} Z &= (\mathrm{const}) \int D[c, c^*] \exp(-S) \, , \\ S &= \int_0^{\beta} d\tau \left[\sum_i c_{i\alpha}^{*} (\partial_\tau - \mu_0) c_{i\alpha} + H \right] . \end{aligned} \tag{2}$$

Here, the electron operators have been replaced by anticommuting Grassmann variables satisfying $c(\beta) = -c(0)$. Arranging the fermions into two types of spinors at each site $\psi = (c_1, c_2)$ and $\chi = (c_1, c_2^*)$, the interaction term can be decomposed into six possible order parameters since

$$6 n_\uparrow n_\downarrow = -(\psi^{\dagger} \sigma \psi)^2 = (\chi^{\dagger} \sigma \chi)^2$$

corresponding to spin and charge fluctuations where σ_a are the three Pauli matrices normalized to $\sigma^{\dagger a} \sigma^a = \sigma^a \sigma^a = 1$ for any a. From the definition of χ, we find that $\chi^{\dagger} \sigma^z \chi$ is just the usual charge density $\psi^{\dagger} \psi$ whereas $\chi^{\dagger} \sigma^x \chi$ and $\chi^{\dagger} \sigma^y \chi$ are the real and imaginary components of the usual BCS order parameter $c_1 c_2$. For positive U, the relevant degrees of freedom include the spin fluctuations along with the charge density $\chi^{\dagger} \sigma^z \chi$, whereas, for the negative-U model, all of the charge order parameters and the total angular-momentum mode $\psi^{\dagger} \sigma_z \psi$ are important. Therefore, the methodology of this

paper at finite doping can be applied to the negative-U Hubbard model in an external magnetic field since the chemical potential becomes an external magnetic field along the z direction for the χ states. For the case of a magnetic Mott insulator it is convenient to decompose the Hubbard term using four Hubbard-Stratonovitch fields ϕ_i^a, $a=x, y, z$, and ρ_i at each lattice site i corresponding to the three spin components and the charge density

$$\exp-\left[\int_0^\beta d\tau\, U\sum_i n_{i\uparrow}n_{i\downarrow}\right] = (1/\mathcal{N})\int D[\phi^a,\rho]\exp\left[-\int_0^\beta \mathcal{L}\, d\tau\right], \tag{3}$$

$$\mathcal{L}=\sum_i [\rho_i^2+\phi_i^a\phi_i^a+\alpha\rho_i\psi_i^\dagger\psi_i+\gamma\phi_i^a(\psi_i^\dagger\sigma_a\psi_i)] .$$

Here, $\mathcal{N}$ is a normalization constant and the Gaussian fields satisfy periodic boundary conditions in τ given by $\rho_i(\beta)=\rho_i(0)$. Although an independent coupling constant for each order parameter could be assigned, our choice is symmetric in the x, y, z spin directions. The remaining coupling constants are constrained to $3\gamma^2-\alpha^2=2U$. Although the full path integral does not depend on which of the infinitely many choices for the couplings we choose, only the choice $\alpha^2=\gamma^2=U$ corresponds to an arrangement of the loop expansion which, at the saddle point, reproduces the correct Hartree-Fock solution for the energy and the SDW insulator gap. For convenience, we specifically choose $\alpha=\gamma=\sqrt{U}$. Moreover, the above choice captures the massless spinwave modes and the massive charge modes as we shall discover in Sec. IV. Our choice of decomposition is thus dictated by the requirement of generating a loop expansion about a specific mean field. Other mean fields such as charge-density waves or Fermi liquids, in general, require other decomposition schemes in order to reproduce the correct Hartree-Fock result.

We can rescale $\rho_i,\phi_i^a\to\sqrt{U}\,\rho_i,\sqrt{U}\,\phi_i^a$ and define the matrix

$$M_i^{\alpha\beta}(\tau)=\rho_i(\tau)\delta^{\alpha\beta}+\phi_i^a(\tau)\sigma_a^{\alpha\beta} .$$

For the effective action, we make the Fourier transformation

$$\psi_i(\tau)=(1/\sqrt{L})\sum_{k,n}\exp(i\mathbf{k}\cdot\mathbf{r}_i-iw_n\tau)\psi_{k,n} ,$$

where L is the number of sites and the Matsubara frequency is $w_n=(2n+1)\pi/\beta$. For the order-parameter fields, we make a similar Fourier transform but require $w_n=2n\pi/\beta$. The partition function is now

$$Z=(1/\mathcal{N})\int D[\psi^\dagger,\psi,\rho,\phi]\exp(-S)$$

with

$$S=(U/2)\mathrm{Tr}(M^\dagger M)+\psi^\dagger(K+UD/\sqrt{L})\psi , \tag{4}$$

where the summations over frequencies, momenta, and internal indices is implied. The inverse electron propagator is

$$K_{pq,nm}^{\alpha\beta}=\delta^{\alpha\beta}\delta_{pq}\delta_{nm}\Delta_{p,n}^{-1}$$

where

$$\Delta_{p,n}^{-1}=(-iw_n+\varepsilon_p-\mu_0)$$

and

$$\varepsilon_p=-2t(\cos p_x+\cos p_y) ,$$

the lattice constant being set to $a_0=1$. Likewise, the order-parameter matrix is given by $D_{pq,nm}^{\alpha\beta}\equiv M_{p-q,n-m}^{\alpha\beta}$ in momentum space.

Integrating out the fermions, we obtain the Landau-Ginzburg action for the order-parameter fields,

$$Z=(1/\mathcal{N})\int D[\rho,\phi]\exp(-S_{\mathrm{eff}})$$

with

$$S_{\mathrm{eff}}=-(\beta UL/2)/\mathrm{Tr}(M^\dagger M) +\mathrm{Tr}\ln(1+UK^{-1}D)+\mathrm{Tr}\ln K . \tag{5}$$

Here, we have rescaled $M\to\sqrt{L}M$. The decomposition of the Hubbard interaction respects the original U(2) symmetry of the Hubbard model realized via $\psi\to V\psi$ and $M\to VMV^\dagger$ with V any element of U(2) and, hence, the terms that appear in the effective Lagrangian to each order in M are restricted. The contribution to the effective action to order n is given by

$$\mathrm{Tr}\ln(1+UK^{-1}D)=-(-U)^n\mathrm{Tr}(K^{-1}D)^n/n .$$

Therefore, around the symmetric vacuum, this defines a perturbation series in U/t since $K\sim t$. For $n=1$, the trace becomes

$$U\,\mathrm{Tr}(K^{-1}D)=2U\rho_{0,0}\sum_{p,m}\Delta_{p,m}$$

which can be eliminated by shifting ρ_i appropriately. To quadratic order, the effective action is given by

$$U\beta L\sum_{k,n}[1+A(k,n)](\phi_{k,n}^{a*}\phi_{k,n}^a+\rho_{k,n}^*\rho_{k,n}) ,$$

where the one-loop contribution is

$$A(k,n)=(U/L\beta)\sum_{p,m}\Delta_{p,m}\Delta_{p+k,n+m} .$$

The physical spin susceptibility[11] of the paramagnetic state is related to the one-loop action by the equation

$$A(k,n)=-U\chi(k,n) .$$

Since the static piece of $A(k,n=0)$ gives the one-loop mass of the fluctuations, we find that they are all degenerate and given by

$$m_q=1+(U/L)\sum_p[f(\varepsilon_{p+q})-f(\varepsilon_p)]/(\varepsilon_{p+q}-\varepsilon_p) .$$

Due to the Van Hove singularity for the square lattice, we find $m_q<0$ for any U/t when $q=Q_0=(\pi,\pi)$, thus spelling an instability towards a new ground state in the Landau-Ginzburg theory. The mass condition is consistent with the usual random-phase-approximation (RPA) susceptibility criterion $U\chi(Q_0)=1$ for a com-

mensurate spin-density wave. However, since the masses of the charge and spin fluctuations are degenerate, there is also an instability into a commensurate charge-density wave which is entirely a product of our particular decomposition of the Hubbard interaction.[12] Each instability corresponds to a saddle-point minimum about which an expansion can be made. Since the copper-oxide superconductor is an antiferromagnet at zero doping, we discard the charge-density-wave (CDW) solution which would, in fact, be relevant for very small U. The correct energetics of the CDW phase requires an alternate Hubbard-Stratonovitch decomposition. For large U, we will establish that the SDW solution itself is stable locally as we must. Through the use of trace formulas, it is easy to obtain the contribution to the Landau-Ginzburg function for any Fourier components of the order parameters to any order n, however, the convergence of such an expansion is poor for $U > t$.

The instability in the Landau-Ginzburg functional implies that the SO(3) subgroup of the full symmetry must be dynamically broken at half-filling due to correlation effects. When a weak interlayer coupling is incorporated, this symmetry breaking has a finite critical temperature which is mimicked by a mean-field theory of the 2D model. Thus, we are instructed to start again with Eq. (4) but instead to shift the fields $M=\overline{M}+\hat{M}$ into mean-field and fluctuation parts. At finite filling, a general magnetic mean-field configuration can be parametrized by $\bar{\rho}_i=\rho_0$ corresponding to a uniform charge density and

$$\bar{\phi}_i^x - i\bar{\phi}_i^y = S\exp(\mathbf{Q}\cdot\mathbf{r}_i)$$

corresponding to any single-wave-vector magnetic state lying on a plane. For $\mathbf{Q}=\mathbf{Q}_0$ and $\bar{\rho}_i=\frac{1}{2}$, this corresponds exactly to a classical spin-S antiferromagnet oriented along the x direction in spin space. Similarly, column states are described by $\mathbf{Q}=(0,\pi)$, ferromagnetism by $\mathbf{Q}=(0,0)$, zone states by $\mathbf{Q}=(Q_x,\pi)$, and finally spiral states by $\mathbf{Q}=(Q_x,Q_y=Q_x)$. The zone states being antiferromagnetically ordered in the y direction and spiralling in the other can be thought of as half-spirals. Due to the reflection symmetries of the square lattice, the partition function is symmetric under any reflection of $\mathbf{Q}$ with respect to the x axis, the y axis, or the $x=\pm y$ axes. Along with the lattice periodicity, this implies a twofold degeneracy for the column states $(0,\pi)$ or $(\pi,0)$, a fourfold degeneracy for the spiral and zone states, and an eightfold degeneracy for any other state. Since these discrete spatial symmetries are unrelated to the SO(3) symmetries of the order parameters, they represent extra degeneracies orthogonal to the Goldstone modes that result from symmetry breaking.

The saddle-point approximation for the order-parameter fields is equivalent to canonical Hartree-Fock (HF) theory. In the latter method, the on-site interaction, now understood to be a 4-fm operator, is expanded around a self-consistent HF ground state

$$n_{i\uparrow}n_{i\downarrow}\rightarrow\langle n_{i\uparrow}\rangle n_{i\downarrow}+n_{i\uparrow}\langle n_{i\downarrow}\rangle-\langle S^+\rangle S_i^- - S^+\langle S_i^-\rangle + \langle S^+\rangle\langle S_i^-\rangle - \langle n_{i\uparrow}\rangle\langle n_{i\downarrow}\rangle \ , \tag{6}$$

where $S^+=c_\uparrow^* c_\downarrow$ and $S^-=(S^+)^\dagger$. Further defining the operators $2Q_i=\psi_i^\dagger\psi_i$ and $2S^a=\psi_i^\dagger\sigma^a\psi_i$, we have $S_i^\pm=S_i^x\pm iS_i^y$. For the Hartree-Fock-Bogoliubov approximation, an additional Wick contraction $\langle c_\uparrow c_\downarrow\rangle$ and its conjugate would be included. Defining c-number fields $\rho_i=\langle Q_i\rangle$ an $\phi_i^a=\langle S_i^a\rangle$, the expectation value for the double-occupancy operator can be expressed as

$$\langle n_{i\uparrow}n_{i\downarrow}\rangle=\rho_i^2-\phi_i^a\phi_i^a \ .$$

The mean-field Hamiltonian is now given by

$$H_{\mathrm{MF}}=-t\sum_{ij}\psi_i^\dagger\psi_i+U\sum_i\psi_i^\dagger(\rho_i-\phi_i^a\sigma^a)\psi_i \ , \tag{7}$$

where the quadratic terms in the c-number fields have been omitted since they are irrelevant to the calculation of any Green's functions. Since the sign of the linear term in $\mathcal{L}$ [Eq. (3)] can be equally chosen $\alpha=-\gamma=\sqrt{U}$, the two electronic Hamiltonians are equivalent. For any planar magnetic state where at least $\bar{\phi}_i^z$ vanishes, the spectrum of H_{MF} is symmetric around zero energy since H_{MF} is manifestly odd under the particle-hole transformation $\psi_{i\alpha}\rightarrow\psi_{i-\alpha}^*$. Likewise, for $x-z$ planar states where at least $\bar{\phi}_i^y=0$, H is odd under the particle-hole transformation $\psi_{i\alpha}\rightarrow\psi_\alpha^*$. Within our representation of the SO(3) algebra, only in these two broad cases will the quasiparticle bands have a particle-hole symmetry. The experimental implication of this is that the physics of planar magnetic states is symmetric with respect to electron and hole doping. However, for topological backgrounds like solitons or merons where all three spin components are nonzero, particle-hole symmetry is explicitly broken.

The inverse of the electron propagator in the broken vacuum is $\overline{K}=K+U\overline{D}$. Integrating out the fermions again, the loop expansion obtained is $(-U)^n(\overline{K}^{-1}\hat{D})^n/n$. For $U>t$, $\overline{K}\sim(U\overline{D})$, and $\overline{D}$ is just the on-site magnetization S, so

$$(-U)^n\mathrm{Tr}(\overline{K}^{-1}\hat{D})^n\sim 1/S^n \ .$$

Since this is not satisfactory for the spin-half case nor for $U\sim t$, we extend the formalism to fermions of arbitrary spin s, where s is some half-integer. This can be accomplished by replacing the doublet ψ by a $2s+1$ column matrix with components $\psi_s,\psi_{s-1},\ldots,\psi_{-s+1},\psi_{-s}$ and exchanging the Pauli matrices for a $(2s+1)$-dimensional irreducible representation of the SO(3) algebra

$$[\sigma^a,\sigma^b]=2i\varepsilon^{abc}\sigma^c \ .$$

At half-filling or one fermion site, the ground state will be a spin-s anteferromagnet giving $S\sim s$ and, hence, the expansion converges in powers of $1/s$. While some properties can be computed surprisingly well[13] in this limit even for spin one-half, we expect that the true ground state for all but very small doping will require an estimate of the fluctuation effects. Rewriting the Hubbard interaction in the SO(3) symmetric fashion as we have done also allows for a $1/N$ expansion where N represents the number of spin doublets.[14] We introduce N_f flavors of spin doublets $\psi_\alpha\rightarrow\psi_\alpha^a$ with $a=1,2,\ldots,N_f$ and $\alpha=1,2$ which will require extending the Pauli matrices to reducible $2N_f$-dimensional matrices having the same commutation alge-

bra but with normalization $\{\sigma^a,\sigma^b\}=2N_f\delta^{ab}$. Since half-filling now corresponds to N_f electrons per site, the total spin becomes $s=N_f/2$ in the antiferromagnetic state. The saddle-point consistency will naturally require that $S\sim s$, again making the loop expansion convergent in powers of $1/N_f$. The expansion is thus convergent for any U/t as long as $US\gg t$. Although the powers of S that appear in the loop expansion are easy to obtain with either expansion, it can be shown that any Green's function or response function can also be organized as an expansion in $1/S$ once the desired calculation is done in the broken state. We will develop the expansion in $1/N_f$ since it requires a simpler representation of the σ^a matrices.

III. PHASE DIAGRAM

Even with an expansion parameter for the Hubbard model, our choice of the background magnetic state is restricted by the invertibility of $\bar{K}$ or equivalently the diagonizability of $H_{\rm MF}$. For a system of finite size, the inverse of $\bar{K}$ can be numerically evaluated[15] for any choice of $\bar{M}$; however, for infinite systems, the choices for $\bar{M}$ become restricted to the planar magnetic states considered above. In the SO(3) broken phase, we have

$$Z=(1/\mathcal{N})\int D[\rho,\phi]\exp(-S_{\rm eff})$$

with $S_{\rm eff}$ given by

$$S_{\rm eff}=\frac{U\beta L}{2}{\rm Tr}[(\bar{M}+\tilde{M})^\dagger(\bar{M}+\tilde{M})] -N_f{\rm Tr}\ln\bar{K}+N_f\sum_n(-U)^n{\rm Tr}(\bar{K}^{-1}\tilde{D})/n\ . \quad (8)$$

Defining a new Nambu spinor $\psi_{p,n}=(c_{\uparrow p+Q,n},c_{\downarrow p,n})$, the propagator matrix $\bar{K}^{-1}$ for any flavor in the SDW background becomes

$$\bar{K}^{-1}_{q,r;m,l}=\delta_{ml}\delta_{qr}G_{q,m}\begin{bmatrix}\Delta^{-1}_{q,m} & -US\\ -US & \Delta^{-1}_{q+Q,m}\end{bmatrix}. \quad (9)$$

Here, $G_{q,m}=[\Delta^{-1}_{q,m}\Delta^{-1}_{q+Q,m}-(US)^2]^{-1}$ and the chemical potential μ_0 is replaced by $\mu=\mu_0+U\bar{\rho}$. At the saddle point, terms linear in the fluctuations $\tilde{M}$ must cancel, from which we obtain

$$\bar{\rho}=(UN_f/2L\beta)\sum_{k,n}G_{k,n}(\Delta^{-1}_{k,n}+\Delta^{-1}_{k+Q,n})\ ,$$
$$1=-(UN_f/L\beta)\sum_{k,n}G_{k,n}\ . \quad (10)$$

$G_{k,n}$ can be factored into

$$[(z_n-E^+_k+\mu)(z_n+E^-_k+\mu)]^{-1}\ ,$$

where $z_n=iw_n$ and the quasiparticle poles located at

$$2E^\pm_k=\varepsilon_k+\varepsilon_{k+Q}\pm[(\varepsilon_k-\varepsilon_{k+Q})^2+4(US)^2]^{1/2}\ . \quad (11)$$

From the particle number constraint $\langle N\rangle=LN_f(1-\delta)$ for doping δ and the canonical expression

$$\langle N\rangle=-(N_f/\beta)\sum_{k,n}{\rm Tr}[\bar{K}]\ ,$$

we identify $-2\bar{\rho}=N_f(1-\delta)$. The sums over the Matsubara frequencies are converted into a sum over the quasiparticle residues giving the usual Hartree-Fock equations for μ and S:

$$4\pi^2(1-\delta)=\int d^2k(f^+_k+f^-_k)\ , \quad (12a)$$

$$4\pi^2=UN_f\int d^2k(f^-_k-f^+_k)/(E^+_k-E^-_k)\ . \quad (12b)$$

Here, $f^\pm_k=\{\exp[\beta(E^\pm_k-\mu)]+1\}^{-1}$ is the Fermi function and the integrals are to be performed over the range $(-\pi,\pi)$ for $\mathbf{k}$. The total energy of the system can be brought to the form[16]

$$E=-(N_f/\beta)\sum_{k,n}(iw_n+\varepsilon_k+\mu_0)\Delta^{-1}_{k+Q,n}G_{k,n}\ .$$

Performing the frequency sum, we find

$$4E/LN_f=4US^2+U(1-\delta)^2 +\pi^{-2}\int d^2k(E^+_kf^+_k+E^-_kf^-_k)\ , \quad (13)$$

which is just the canonical Hartree-Fock energy for a general SDW state. At half-filling and $US>t$, it is easy to verify that the gap equation reads $S\sim N_f/2$. The term in the loop expansion of order n in the fluctuations is therefore of order N_f^{-n+1} since there is an overall N_f from the loop over fermions just as in the gap equation.

For large enough N_f flavors, the saddle point is an excellent approximation, and we assume that the physics does not alter dramatically when we set $N_f=1$. We have numerically evaluated these equations at zero temperature for $2<U<15$ and doping $0\le\delta\le0.6$ with a mesh of 500×500 points in the Brillouin zone making use of all the symmetries. The quasiparticle states describe two bands each with L states. They are just the eigenstates of $H_{\rm MF}$ [Eq. (7)] in the SDW background with energies $E^\pm_k$. $H_{\rm MF}$ can be diagonalized by the unitary transformation that preserves the anticommutation relations via $\bar{\psi}_k=V(k)\psi_k$, where $V(k)=exp(i\theta_k\sigma^y)$ and

$$\tan(2\theta_k)=2US/(\varepsilon_k-\varepsilon_{k+Q})\ .$$

In terms of the Bogoliubov states $\bar{\psi}=(\alpha_k,\beta_k)$, a general SDW ground state $|\psi\rangle_Q$ can be written in operator form as

$$|\psi\rangle_Q=\prod_{k<k_f}(-\sin\theta_kc^\dagger_{k+Q\uparrow}+\cos\theta_kc^\dagger_{k\downarrow})|0\rangle\ , \quad (14)$$

where k_f is the Fermi momentum. Therefore, the new band states are admixtures of spin-up and spin-down electrons. The top of the lower band occurs at $(\pi-Q_x/2,\pi-Q_y/2)$, whereas the bottom of the upper

band occurs at $(-Q_x/2, -Q_y/2)$ since, by particle-hole symmetry, we have $E_k^+ = -E_{k+Q_0}^-$. The gap between the two bands, or the Mott-Hubbard gap, is

$$\Delta = 2US - 4t\cos(Q_x/2) - 4t\cos(Q_y/2)\ .$$

The Fermi surfaces for the spiral, column, and zone states are shown in Fig. 1. Sprial and zone states have an asymmetric Fermi surface lying entirely in the right-hand quadrant for doping less than a critical doping that depends on U/t whereas column states have a symmetric Fermi surface. The bandwidths for the various states vary between a maximum of $8t$ for the ferromagnetic state and a minimum

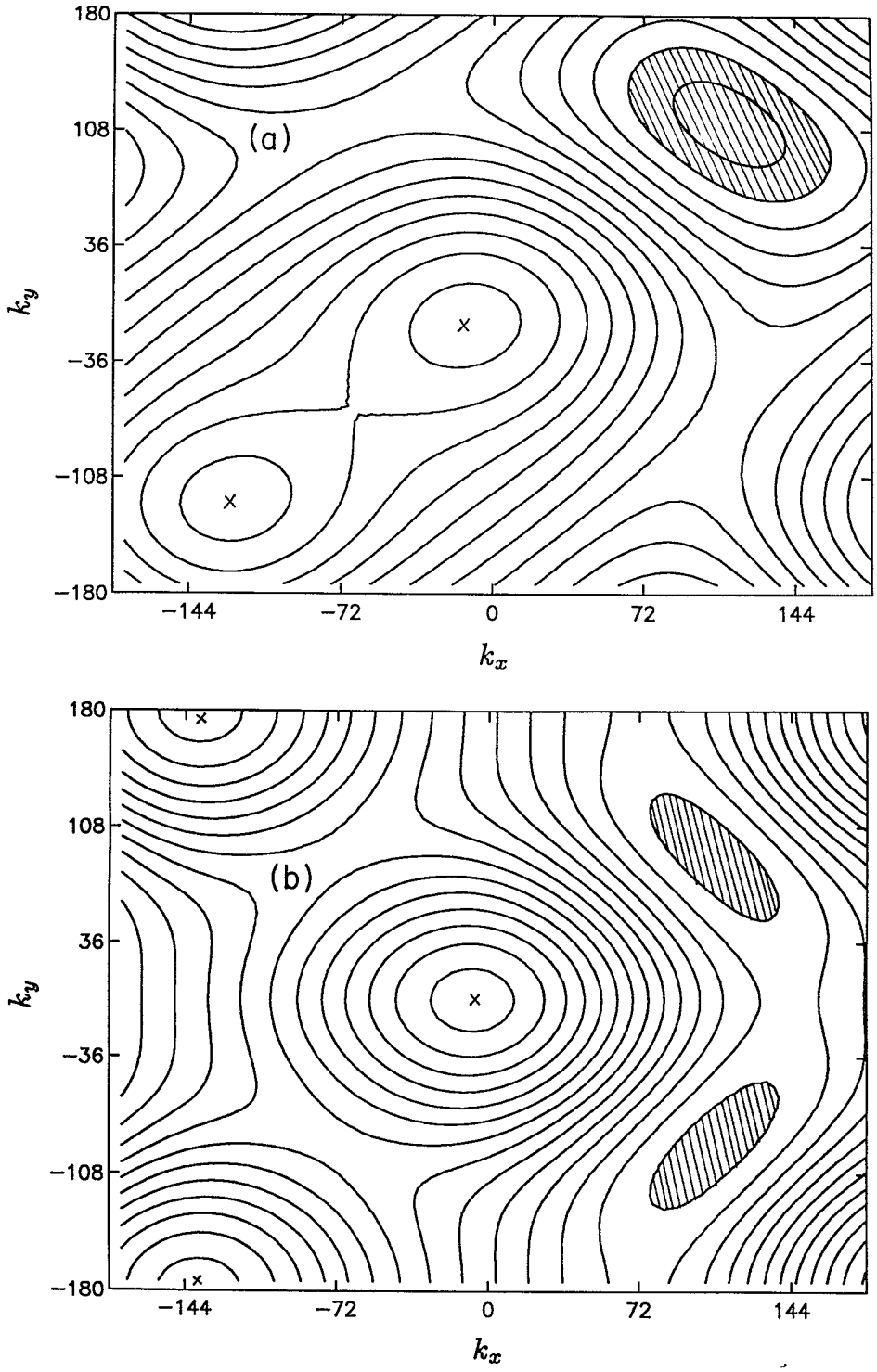

FIG. 1. The energy contours of E_k^- for (a) the spiral state with $Q_x = Q_y = 3\pi/4$, (b) the zone state with $Q_x = 3\pi/4$, and (c) the column state. Shaded regions show pockets of holes at finite doping and the absolute minima are designated by a cross. The large flat regions give rise to two peaks in the spectral density.

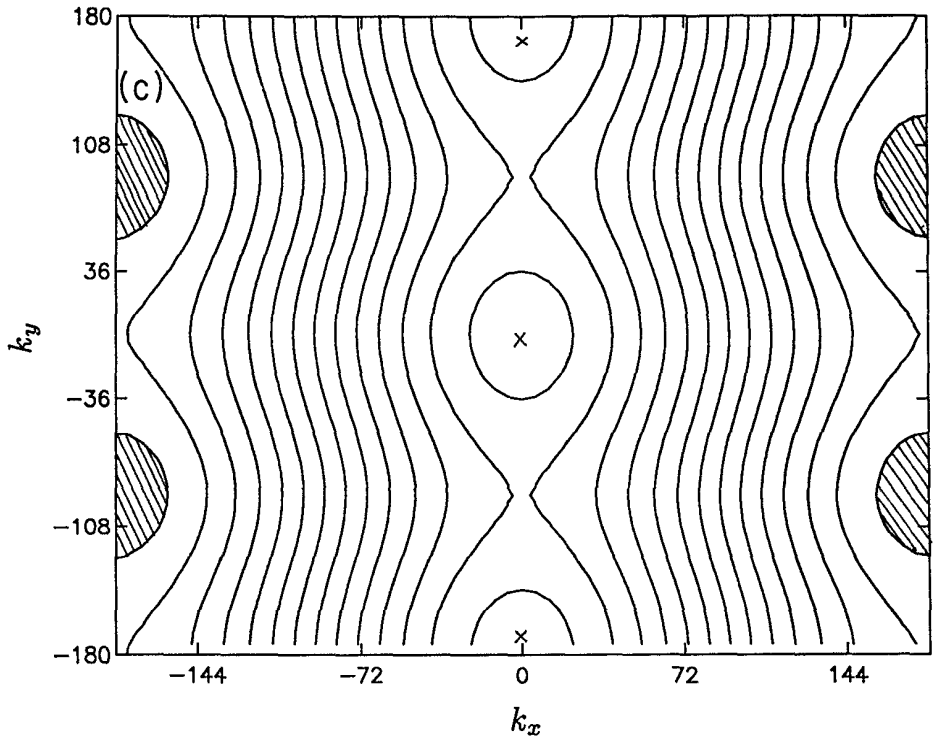

FIG. 1. (*Continued*).

$$[16t^2+(US)^2]^{1/2}-US$$

for the Néel state which approaches $4J$ for $US \gg t$, where $J=4t^2/U$.

There is considerable evidence now that the zero-temperature ground state of the half-filled 2D Hubbard model has long-range magnetic order[17] with an on-site magnetization $S\sim 0.3\hbar$ a value within the range found in μSR measurements.[18] For the range of intermediate of U we studied, the antiferromagnetic state $\mathbf{Q}=\mathbf{Q}_0$ minimizes the energy with the on-site magnetization given by

$$2S=1-2J/U+O(1/U^3) .$$

In contrast, the ferromagnetic state has the highest energy with the self-consistent magnetization $S=\frac{1}{2}$ for $U/t\geq 4$. The values of the energy per site E/L and S derived in the path-integral formulation (Fig. 2) agree exactly with canonical Hartree-Fock methods.[4,19] Finite-temperature effects at the mean-field level are only sizable when the charge gap $\Delta\sim k_B T$, as seen from Fig. 2, where S precipitously falls to zero near $U/t\sim 2$ when $\beta=6/t$. Quantum Monte Carlo (QMC) simulations[17] at the same temperature for a 12×12 system at half-filling give $E/L\sim -1.15t, -0.85t$ for $U/t=2,4$, respectively, slightly lower than the saddle point which has energies $E/L=-1.12t, -0.797t$. Therefore, for small U/t, spin-wave fluctuations are less important. For very large U/t, the energy can be obtained by the effective superexchange Hamiltonian or the $t-J$ model which gives

$$E/L=-4.63(t^2/U)+34.6(t^4/U^3)+O(1/U^5) .$$

This result in the limit of infinite U/t converges to $E/L\sim -1.15J$ whereas the saddle-point result converges to

$$E/L\sim -2t^2/US=-J ,$$

the energy of the Neél state for the $t-J$ model at half-filling. In both extremes of U/t, the mean-field energies are within 13% of the true ground-state energy. From the Hartree-Fock approximation, we obtain vanishing double occupancy at infinite U/t or

$$\langle n_{i\uparrow}n_{i\downarrow}\rangle=(1-\delta)^2/4-S^2 ,$$

which, at half-filling, goes to

$$\langle n_{i\uparrow}n_{i\downarrow}\rangle=J/U-(J/U)^2+O(1/U^4) .$$

Infrared reflectivity experiments[20,21] find a gap $\Delta=2US\sim 2$ eV. The magnetization M inferred from μSR is related to S via $M=g\mu_B S$, where the g factor for the electron is 2.2. In our saddle-point approximation, the values of Δ and S from experiment suggest $U/t\sim 3.3$ and $t\sim 1$ eV. However, spin-wave contributions[19] appreciably depress the value of the self-consistent magnetization S and the quasiparticle gap $2US$, therefore requiring a larger choice of U/t. These corrections will emerge in our treatment when we consider the one-loop action. Instead of fixing these parameters at the mean-field level, which are affected by interlayer couplings as well, we will examine the phase diagram at finite doping over a wide range of U/t.

The Van Hove singularity in the density of states

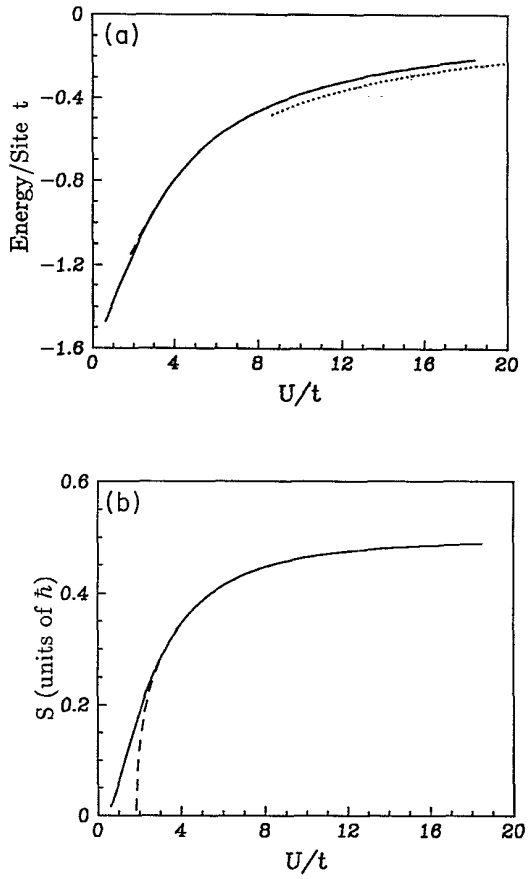

FIG. 2. (a) Energy per site E/L in t eV compared with spin-wave theory (Ref. 17) (dotted line). (b) Self-consistent magnetization S for the antiferromagnetic state at half-filling, the solid line is for $\beta=\infty$ and the dashed line is for $\beta=6/t$. Double occupancy is given by $\frac{1}{4}-S^2$.

(DOS) for $\mathbf{Q}=\mathbf{Q}_0$ occurs at $\pm US$, the upper and lower band edges which, in momentum space, lie along $\pm k_x \pm k_y = \pi$. At very small doping, $\delta \ll 1$ and $U \gg t$, the energy of the antiferromagnetic (AF) state is

$$E_{\mathrm{AF}} \sim -(1/4U\pi^2)\int d^2k\, \varepsilon_k^2 f_k^- \ .$$

In contrast, the two bands for the ferromagnetic state have energy $\varepsilon_k \pm US$ and therefore, exactly at half-filling, the total energy [Eq. (13)] is zero. Slightly away from half-filling, however, the energy of the ferromagnetic state becomes $E_F \propto -4t\delta$. Therefore, in the $U \to \infty$ limit, we find $E_F < E_{\mathrm{AF}}$, similar to the Nagaoka result. At finite U/t and doping, this need not be the case and, in a continuum classical model considered by Shraiman and Siggia,[22] a planar twist near the hole is favored as opposed to the Nagaoka state or a depression in the local magnetization as in the spin bag. At finite doping, the mean-field description of these local twists corresponds to a twisted SDW with $\mathbf{Q} \neq \mathbf{Q}_0$.

There are two parameters of interest as doping is varied, the pitch $\mathbf{q}=\mathbf{Q}_0-\mathbf{Q}$ and the on-site magnetization S. As the pitch is increased from zero, the bandwidth widens and the peak in the DOS moves below the band edge leading to a pocket of holes above the energy $-US$. If we neglect the $\mathbf{q}$ dependence of S by setting $S=\frac{1}{2}$, doping should then induce a transition to $\mathbf{q} \neq 0$. In this approximation, one finds that the pitch varies linearly with doping for small doping and for higher doping unwinds the antiferromagnet to a ferromagnet[23] as shown in Fig. 3 whereas allowing S to depress to its self-consistent value dampens the unwinding. Varying q_x and q_y independently, we find that, for a range of doping and any U/t, the spiral states $q_x = q_y$ have the lowest energy (Fig. 4) reflecting the importance of the specific size and shape of the pocket of holes that develop for each $\mathbf{q}$. In addition to the minimum along the diagonal, a saddle point appears along the zone edge with a relative energy difference of less than 0.5% when $U/t=5$, $\delta=0.05$. As the doping is increased, this difference is narrowed until the zone state becomes the absolute minimum and the spiral state a local minimum, for example, at a critical doping $\delta_{c1}=0.16$ for $U/t=5$.

The energetics of the twisted magnetic states depends critically on the electronic DOS as the $S=\frac{1}{2}$ case showed. In Fig. 5, we plot the DOS of the spiral and zone SDW states near the spiral-zone transition. The two flat regions (four saddle points) in each of the contour plots in Fig. 1 give rise to prominent peaks in the DOS analogous to the Van Hove logarithimic singularity for the paramagnetic state. For the zone states, two peaks of roughly equal size occur for every q_x, which become exactly symmetric located at opposite band edges for the column states when $q_x=\pi$. In contrast, for the spiral states, the peaks are highly asymmetric with the smaller peak which is located deeper in the band, vanishing for $q_x \geq \pi/2$. The first peak near the Fermi surface is the remnant of the peak at the band edge of the Mott-Hubbard band and is deeper in the band for the spiral state than the zone state. Considering these spectral distributions, the transition from spiral states to zone states should occur when the holes can fill the peak near the band edge of the zone state which occurs at δ_{c1}. Since

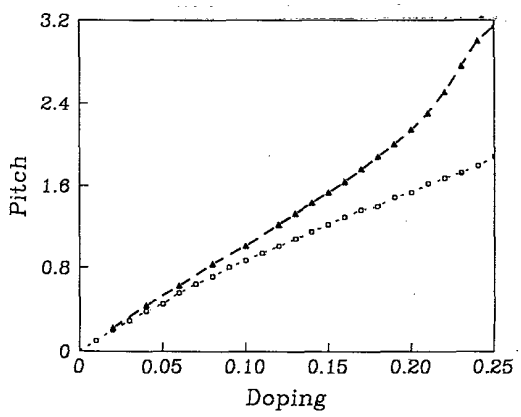

FIG. 3. Doping-induced spiral pitch $q=|Q_0-Q|$ for $S=\frac{1}{2}$ (top curve) and for S determined self-consistently (bottom curve).

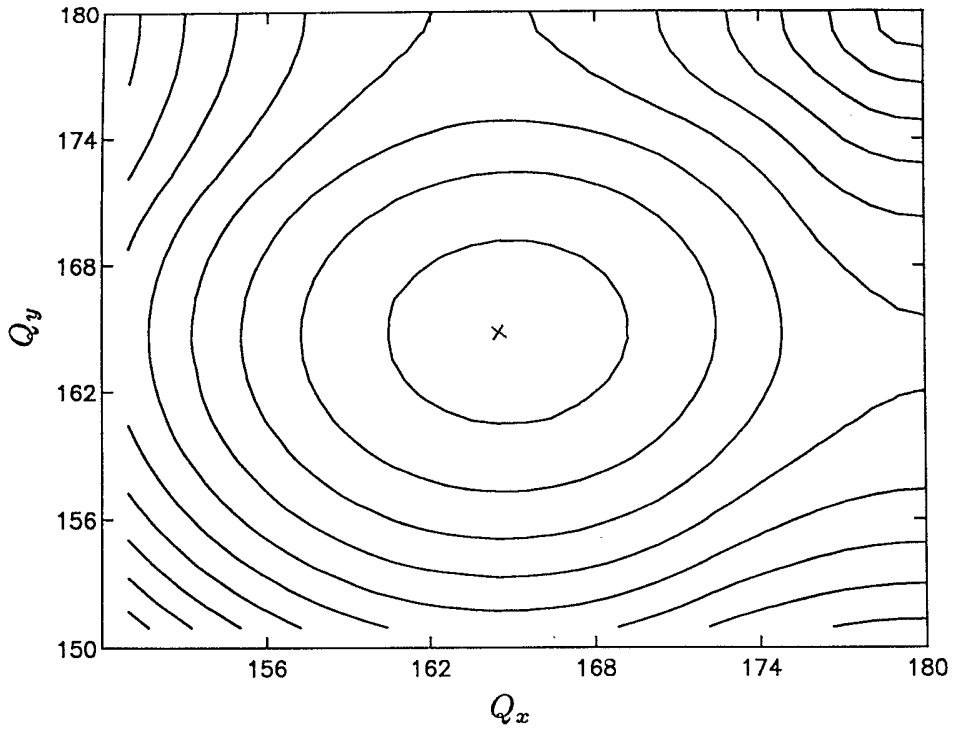

FIG. 4. Contour of the energy per site as a function of the incommensurate wave vector Q for $U/t=5$ and $\delta=0.05$. The minimum is in the center and note the saddle point along the zone edge.

this transition will involve a discontinuous change in the order parameter q, we will consider it to be a first-order magnetic phase transition. For doping beyond the spiral-zone first-order transition, the pitch continues to increase until it reaches π and, hence, this results in a second-order transition line between zone and column states. As U/t is increased, the pitch increases more rapidly with doping and, for $U/t>10$, there is a second-order transition to a ferromagnetic state before the spiral-zone state transition. Therefore, doping the ferromagnetic state at this range of U/t results in a first-order transition into a column phase at δ_{c2}. The intersection of the phase boundaries occurs at a tricritical point between the column phase, the ferromagnetic phase, and a spiral phase at $U/t\sim10$, $\delta\sim\frac{1}{3}$, and another tricritical point between the column phase, a zone phase, and a spiral phase at $U/t\sim9$, $\delta\sim0.31$ as shown in Fig. 6.

At finite doping, the twisted magnetic states are in competition with the paramagnetic metal with no symmetry breaking. For the unbroken phase, $S=\mathbf{Q}=0$, making $E_k^{\pm}=\varepsilon_k$. The particle number constraint becomes

$$1-\delta=(1/2\pi^2)\int d^2k f_k^-$$

and the energy per site is

$$E/L=U(1-\delta)^2/4+(1/2\pi^2)\int d^2k\,\varepsilon_k f_k^- .$$

For large enough doping, namely at δ_{c3}, the twisted zone states are unstable towards a paramagnetic phase where hopping costs no spin-exchange energy. The instability

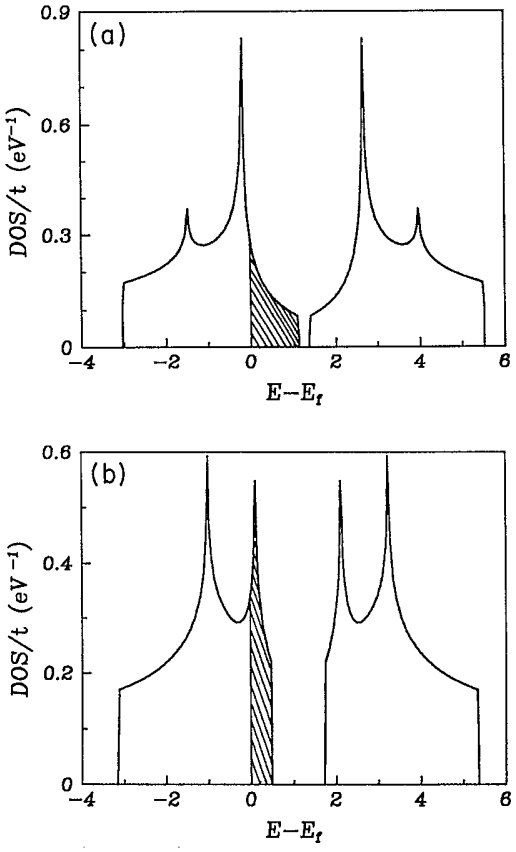

FIG. 5. The density of states in eV^{-1} per site for (a) the spiral state and (b) the zone state precisely at the spiral-zone first-order transition which occurs at $\delta=0.16$ when $U/t=5$. The pocket of holes (shaded region) is to the right of the largest singularity in the lower MH band in (a) and to the left in (b).

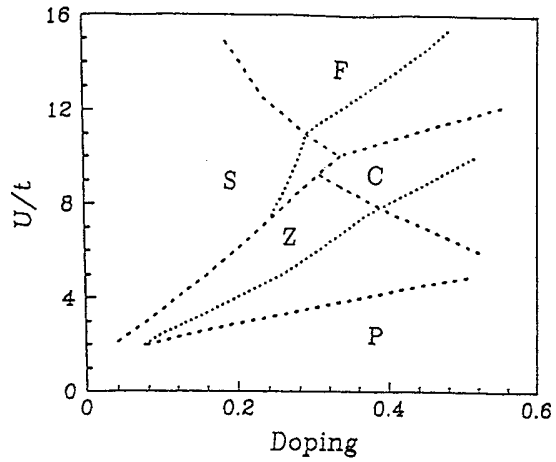

FIG. 6. Phase boundaries with a tricritical point between a ferromagnet (F), a spiral (S), and a column (C) phase at $U/t\sim 10$ and $\delta\sim 1/3$. The zone (Z) states are unstable towards the normal paramagnetic (P) states. The dotted lines are the Mott-Hubbard band crossing lines.

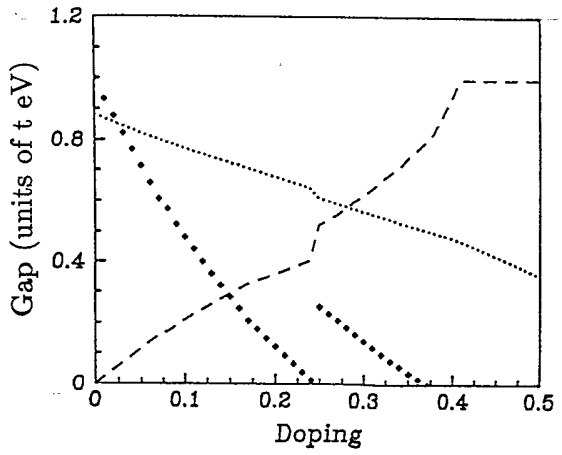

FIG. 7. The charge gap $\Delta=2US-4t\cos(Q_x)-4t\cos(Q_y)$ for $U/t=7.5$ is normalized to the gap at half-filling $6.6t$ (diamonds). Doping reduces the normalized magnetization $2S$ (dotted line) and increases the normalized pitch $(\pi-Q_x)/\pi$ (dashed line); the discontinuity at $\delta\sim 0.25$ reflects the spiral-zone transition.

of the paramagnetic metal to a SDW ordering at a wave vector along the Brillouin zone boundary as the doping is reduced has also been obtained using the Stoner criterion in the weak-coupling limit.[24] In this latter method, it was shown that the instabity appears in the linearly polarized incommensurate SDW channel at $\delta_{c3}\sim 0.143$ when $U=2t$. Considering twisted SDW's alone, however, we find $\delta_{c3}=0.077$. The discrepancy is, in part, due to the difference in the type of SDW considered but is also due to the omission of perturbative corrections to the energy. Since $E_k^{\pm}$ is U independent and S is zero for the paramagnetic state, the fluctuations are perturbative in U and cannot be controlled in our $1/S$ expansion unlike the magnetic mean-field states. These perturbations will move the zone-paramagnetic phase boundary considerably and this may further restrict the doping region for the incommensurate magnetic phases. While earlier Hartree-Fock treatments of the 2D Hubbard model away from half-filling give an entirely different phase diagram consisting only of ferromagnetic, antiferromagnetic, and paramagnetic regions,[25] twisted SDW states provide a compelling electronic structure with singularities in the DOS, pockets of holes, and asymmetric Fermi-surface topologies.

Doping induces frustration of two sorts by reducing the on-site magnetization and increasing the pitch as shown in Fig. 7 for $U/t=7.5$. μSR measurements[26] and neutron diffraction[18] show a rapid supression of the on-site magnetization whereas, at mean field, S is reduced by up to $\frac{3}{4}$ of its original value at half-filling. Like the case of half-filling, spin-wave renormalizations and interlayer couplings must be balanced to obtain the correct reduction in S. The discontinuity in S and the pitch in Fig. 7 is due to the first-order spiral-zone transition. Since Q_y jumps to π at the transition, the net MH gap is higher for the zone states. Frustration through doping leads to a dramatic closure of the MH gap whenever

$$S=2t[\cos(Q_x/2)+\cos(Q_y/2)]/U\ ,$$

which occurs at $\delta=0.07$–0.36 for $U/t=2$–7.5 within the zone states (Fig. 6). At higher $U/t=7.5$–11, the MH gap vanishes at $\delta=0.24$–0.29 within the spiral states. This is followed by a discontinuous reappearance of the gap at the spiral zone which then finally vanishes at $\delta=0.36$–0.57 within the zone-column states. The MH band crossing for $U/t>11$ occurs exactly at $\delta=1-8t/U$ within the ferromagnetic state and another crossing for $U/t<16$ within the column states but at a doping $\delta>0.57$. In contrast, if we fix $S=\frac{1}{2}$, the charge gap vanishes only if $U/t<4$ and $U/t<8$ for zone and spiral states, respectively. The doping-induced depression of S is therefore crucial for the MH band crossing at intermediate and large U/t.

Although the momentum-integrated spectral density has no gaps after the band crossing, the gap between the two bands at the same point k in the Brillouin zone satisfies $E_k^+-E_k^-\geq 2US$ with the minimum separation at $k_x=k_y\pm\pi$ and $k_x=-k_y-Q$ for spiral states. When the MH bands cross, the states at the lower and upper band edges pile up, as displayed in Fig. 8, giving rise to a wide central peak in the density of states which could be related to the broad doping-induced absorption band at 0.5 eV seen in infrared reflectivity data[27] and angle-resolved-photoemission spectra.[28] The position of the central peak relative to the Fermi surface increases with higher doping and U/t and for $U/t=5$ and $\delta=0.30$ is located roughly 1 eV above the Fermi surface. For doping beyond the MH band crossing, the MH gap becomes negative and causes the upper MH band to come arbitrarily close to the chemical potential located in the lower MH band as shown in Fig. 9. The proximity of upper MH band enhances low-energy interband transitions and this

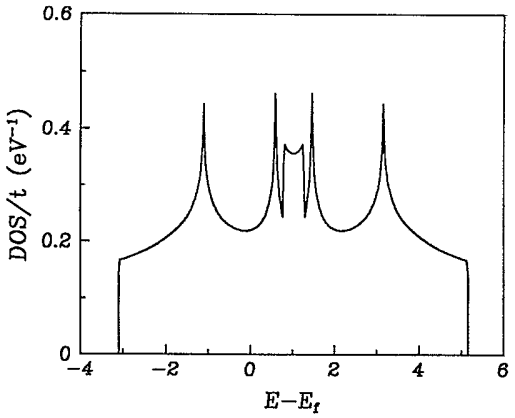

FIG. 8. A new peak appears in the DOS 1 eV above the Fermi surface with a width ~0.5 eV due to the overlap of the upper and lower Mott-Hubbard bands for $U/t=5$ and $\delta=0.30$.

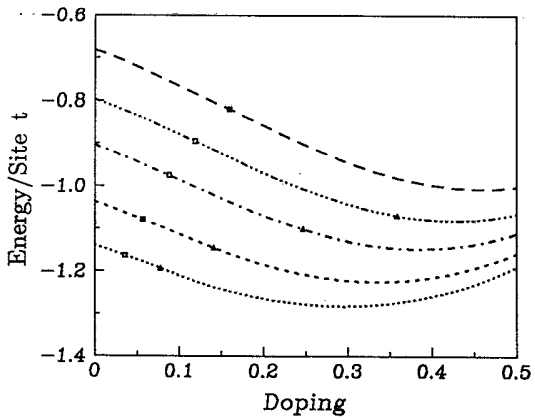

FIG. 10. Energy per site for $U/t=2$, 2.5, 3.25, 4, 5 from bottom to top respectively. Spiral-zone state transitions are indicated by the squares and the zone-parameagnet transitions by triangles. Energy gained per hole at low doping is $\propto -t$.

may be connected to the anomalous deviation of the Hall coefficient from the single-band approximation $R_H \sim 1/\delta$ and the precipitous fall[29] in the doping region relevant to superconductivity. Although these data are qualitatively consistent with the modified band structures for the spiral SDW state, the precise influence of the interband transitions on the transport properties and the optical conductivity will be discussed in a later paper. As we will show, fluctuations about the SDW mean-field theory lead to a substantial modification of any simple effective one-electron-band picture. The resulting coupling of the spin and charge fluctuations must be incorporated for a precise comparison with experiment.

The ground-state energy for the twist states is determined through a competition between the kinetic energy of the holes and the spin-exchange energy of the magnetic background. For $U/t \leq 5$, the energy per site E/L (Fig. 10) decreases almost linearly up to some doping beyond the spiral-zone transition but below the zone-paramagnet transition. As a result, the energy gain per hole

$$E_h \equiv [E(\delta,\mathbf{Q})-E(\delta=0,\mathbf{Q}_0)]/L\delta$$

is of order $-t$ for the twist states as in domain-wall states[30] and in the string picture of Brinkman and Rice. In QMC simulations, E/L is minimized at $\delta \sim 0.27$, 0.38 with values $-1.27t$, $-1.15t$ for $\beta=6/t$. At the same temperature, our mean field gives minimum energies at $\delta=0.30$, 0.43 of $E/L=-1.27t$, $-1.07t$, respectively. Although this comparison will be affected by finite-size effects in QMC, it nevertheless shows that quantitative agreement between mean-field methods and other exact approaches can be obtained through a proper choice of the saddle point.[31] As U/t is increased, the linear dependence of E/L crosses over to a quadratic dependence (Fig. 11) near half-filling making E_h vanish in the $\delta \to 0$ limit. E/L saturates (E_h reaches a minimum) at a higher doping $\bar{\delta}$ and then increases to zero at $\delta=1$ for any U/t. In the absence of any loss of Coulomb screening, a Maxwell construction can be used to demonstrate that phase separation will occur for $\delta < \bar{\delta}$. Phase separation can take place even for $\delta > \bar{\delta}$ if an additional local minimum in E_h occurs at a doping above $\bar{\delta}$ which may occur in the presence of a first-order transition. Evaluating the position of these minima then gives the phase diagram in Fig. 12 which includes an antiferromagnetic-ferromagnetic mixture at large U/t, a antiferromagnetic-spiral and antiferromagnetic-zone mixture at intermediate U/t and an antiferromagnetic-paramagnetic mixture at $U/t < 2.2$. An additional minimum in E_h appears when $2.2 < U/t < 3$, giving rise to a zone-paramagnetic mixture and a spiral-zone mixture in the range $7.6 < U/t < 9$ in the doping region where these first-order transitions occur. Pure spiral phases appear in the region $0.2 < \delta < 0.3$ whereas pure zone phases appear for a much wider range of doping. At large U/t, the antiferromagnetic-ferromagnet mixtures are consistent with dynamical[32] and mean-field[33]

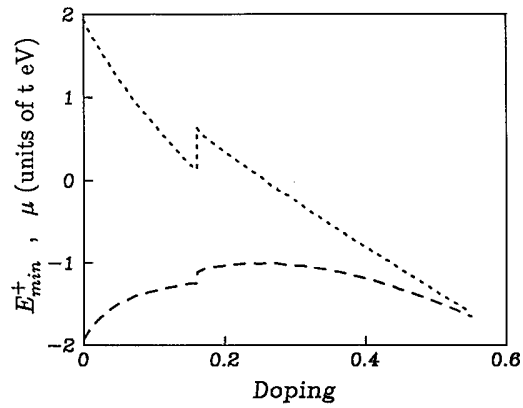

FIG. 9. The bottom of the upper Mott-Hubbard band (upper curve) approaches the Fermi surface (lower curve) as doping is increased. The discontinuity at $\delta=0.16$ for $U/t=5$ reflects the spiral-zone transition.

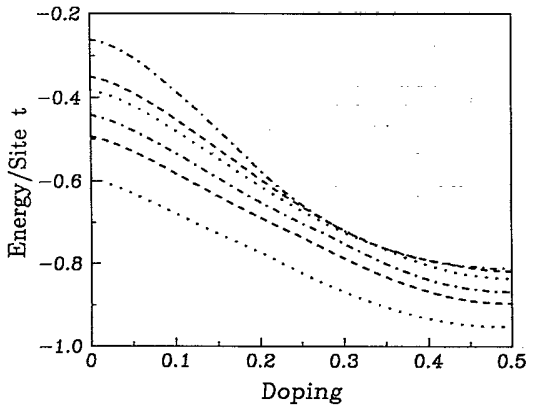

FIG. 11. Energy per site for $U/t=6$, 7.5, 8.5, 10, 11, 15 from bottom to top, respectively. The increasing convexity with U/t favors phase separation at the mean-field level.

calculations for the t-J model. The phase-separated regions not only differ magnetically but also electronically due to the variation of the charge gap with doping. However, the precise connection of these phase mixtures to the inhomogeneities observed in superconducting samples[34] will require an understanding of the Coulomb energies of the phase-separated regions, interfacial effects, and the induced reordering of mobile oxygen atoms.

In Sec.II, we provided a Landau-Ginzburg expansion for the SO(3) symmetric vacuum perturbative in U/t. At weak coupling $U<t$, this expansion can be truncated at quartic order and the energetics of any mean-field solution compared. Perturbative expansions of this type[24] favor a linearly polarized incommensurate SDW rather than a twisted state. A linearly polarized incommensurate SDW can be written as a super-position of two twist states, one at $\mathbf{Q}$ and the other at $-\mathbf{Q}$ giving $\bar{\phi}_i^a = S\cos(\mathbf{Q}\cdot\mathbf{r}_i)$ for some component a and all other components vanishing. Just as the commensurate SDW at half-filling gaps the Fermi surface everywhere along $\pm k_x \pm k_y = \pi$, the incommensurate linear SDW also gaps the Fermi surface more evenly than the single twist states.[35] Therefore, at least for small repulsion U, the linearly polarized SDW should be the ground state away from half-filling. However, for $U \geq t$, the energetics is no longer dominated by the electronic DOS near the Fermi level alone. This is evident in Fig. 5 where it is shown that the DOS well within the band is dramatically affected by the magnetic configuration. Even in the presence of more than one wave vector $\mathbf{Q}$, a mean-field estimate of the energy per site of linearly polarized SDW states[36] gives an energy per site

$$E(\delta)-E(\delta=0)\sim -0.014t$$

at $\delta\sim 0.185$. The twisted SDW, meanwhile with just one wave vector, has considerably lower energy

$$E(\delta)-E(\delta=0)\sim -0.16t\ .$$

Moreover, the holes in linearly polarized SDW states preferentially move where the magnetization $\bar{\phi}^a\sim 0$, that is, along lines perpendicular to $\mathbf{Q}$ as various lattice calculations show.[15,36] For large U/t, this can be understood from the requirement that double occupancy vanish, which implies $\rho_i^2 \sim S^2\cos^2(\mathbf{Q}\cdot\mathbf{r}_i)$. Including long-range Coulomb repulsion, the stability of such a nonuniform charge distribution is even less likely. In contrast, for twist states, the magnetization, the pitch, and the hole density are uniform.

The finite density of states at the Fermi surface in the lower Hubbard band makes the twist states metallic away from half-filling (e.g., Figs. 5 and 8). However, due to the significant rearrangement of these states, the DOS at the Fermi surface $\rho(\varepsilon_f)$ is considerably lower than the metal with no symmetry breaking. Naturally, for the insulating commensurate SDW, $\rho(\varepsilon_f)=0$, which increases very rapidly upon doping and soon reaches a maximum within the spiral states (Fig. 13). Further doping only reduces

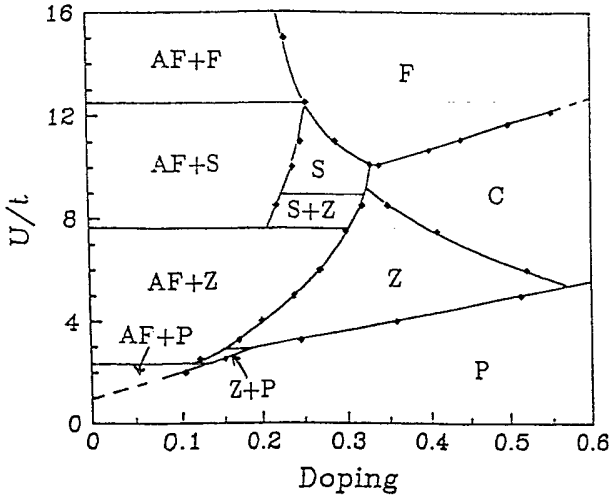

FIG. 12. Phase separation occurs for $\partial^2 E/\partial\delta^2<0$ evaluated using Fig. 11 and 12. The phases are spiral (S), zone (Z), column (C), and ferro-, antiferro-, and paramagnetism (F,AF,P).

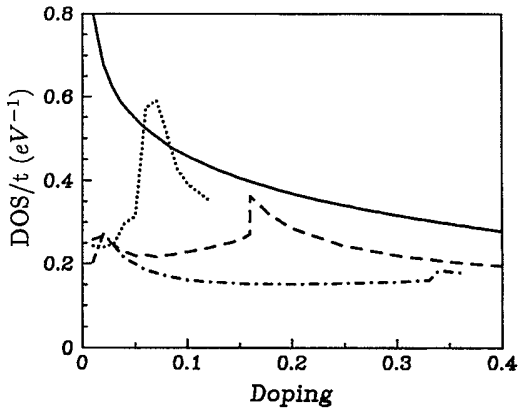

FIG. 13. Density of states at the Fermi level in eV^{-1} per site is higher for a paramagnetic metal (solid line) with $U=0$ than the twisted magnetic metal; $U/t=2.5$, 5, 10 is shown as dotted, dashed, and dot-dashed.

$\rho(\varepsilon_F)$ at the expense of a growing number of states deeper in the band. At the spiral-zone transition, $\rho(\varepsilon_F)$ increases abruptly due to a translation the first peak towards the bandedges. The increase in $\rho(\varepsilon_F)$ is smaller for increasing U/t. When the system becomes paramagnetic, $\rho(\varepsilon_F)$ again abruptly increases. Except for a small region of doping at $U/t=2.5$, $\rho(\varepsilon_F)$ for the twist states is always lower than the system with no symmetry breaking.

At the saddle-point level, the physical picture is that of a collection of essentially noninteracting quasiparticles in an effective single-particle density of states corresponding to a twisted SDW. Fluctuation corrections will give rise to significant corrections to this picture. The most significant of these, as we will show, is the coupling of charge fluctuations to the twist degrees of freedom of the background SDW. This will affect experimental response functions such as the magnetic susceptibility χ_m. In addition to the spin-wave contributions, an electron Pauli contribution will arise from charge-spin coupling. A meaningful evaluation of χ_m must therefore be performed at the one-loop level beyond the saddle point. In contrast, the effective one-electron picture allows a reasonable approximation to the plasma frequency $\hbar\omega_p$ which may be written[37]

$$(\hbar\omega_{px})^2=(2e^2/\pi d)\int d^2k\,(\nabla_{k_x}E_k^-)^2\delta(E_k^- -E_f)\ .$$

Here, $d=13.7$ Å, the interlayer spacing for the lanthanum perovskites. For the zone states, the group velocities are asymmetric, $\hbar\omega_{px}\neq\hbar\omega_{py}$, so we define the rms plasma frequency $\omega_p^2=\omega_{px}^2+\omega_{py}^2$. The plasmon energy for $U/t=2.5$, 5, 10 is displayed in Fig. 14. Increasing the interaction strength U lowers the plasmon energy for all dopings consistent with the redistribution of spectral weight from the Fermi surface into interband transitions to the upper MH band and other bands omitted in the Hubbard model. At the sprial-zone transition, the increase in $\rho(\varepsilon_F)$ is reflected by a jump in the plasmon energy therefore enhancing the Drude conductivity. Despite the discontinuity, the plasmon energies saturate to values

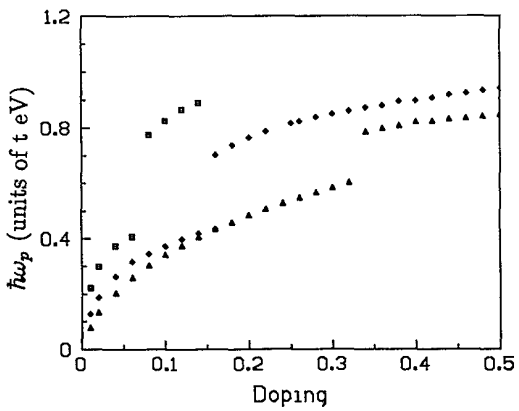

FIG. 14. Plasmon energy $\hbar\omega_p$ in eV for $U/t=2.5$, 5, 10 plotted with squares, diamonds, and triangles, respectively. The discontinuity is due to the spiral-zone transition.

of $\hbar\omega_p\sim0.8$–1.0 eV, in reasonable agreement with infrared reflectivity data.[38] This is in contrast to nonmagnetic one-electron-band models which predict much larger values for the plasma frequencies.[37] Since the experimentally derived values are subject to ambiguities in extracting the Drude portion of the conductivity, we conclude that the doping dependence of $\hbar\omega_p$, rather than its absolute value, places a stronger constraint on theory.[39] Our mean-field twist states have the correct saturation at higher doping, but the rapid increase below the spiral-zone transition, which can be parametrized as $\hbar\omega_p\sim\sqrt{\delta}$, is more difficult to experimentally verify. Although phase separation could smear out the spiral-zone transition, the dramatic difference in $\hbar\omega_p$ for the spiral and zone states for $U/t<10$ at low and high dopings, respectively, is a new prediction. The plasmon energy is insensitive to the interaction effects that determine the scattering time τ_{sc} and the resulting dc conductivity. The band Fermi-liquid picture inherent in these mean-field calculations, while including correlation effects through S and $\mathbf{Q}$, entirely neglect the coupling of massless spin waves to charge-density fluctuations. These effects are crucial in determining τ_{sc} and may, in fact, be more important than the resistivity due to electron-phonon scattering.

The interaction effects that are included at mean field give a finite quasiparticle weight Z_k to particle-hole pairs near the Fermi surface. Z_k is exactly related to the discontinuity in the momentum distribution function[40]

$$n_k=-\langle c_{k\alpha}^*(\tau)c_{k\alpha}(0)\rangle_{\tau\to0^+}$$

at the noninteracting Fermi surface. Taking into account the momentum translation between the c_k fields and the propagator matrix for the ψ_k fields [Eq. (9)], the up-spin contribution is

$$n_{k\uparrow}=\sum_{w_n}\Delta_{k+Q,n}^{-1}G_{k,n}\exp(iw_n\tau)\ .$$

At zero temperature, the upper band contribution vanishes, giving

$$n_{k\uparrow}=[(E_k^- -\varepsilon_{k+Q})/(E_k^- -E_k^+)]f_k^- \tag{15}$$

for the SDW background. For $\mathbf{Q}=\mathbf{Q}_0$, this reduces to $n_{k\uparrow}=(1-\varepsilon_k/E_k^+)/2$. Although the Fermi surfaces for spiral SDW states are asymmetric (Fig. 1), the crystal momentum

$$\mathbf{J}_q\sim\sum_k\langle c_{k+q\alpha}^*(\tau)\nabla\varepsilon_{k+q/2}c_{k\alpha}(0)\rangle_{\tau\to0^+}$$

vanishes. This occurs in light of the fact that the change in the Fermi surfaces of the up- and down-spin electrons occurs in opposite regions of the Brillouin zone expressed by the identity $n_{k\uparrow}=n_{-k\downarrow}$. This implies that

$$\mathbf{J}_q\sim\delta(\mathbf{q})\sum_k\nabla\varepsilon_k(n_{k\uparrow}+n_{k\downarrow})=0\ .$$

Making use of this identity, we find $n_k=n_{k\uparrow}+n_{-k\uparrow}$, which has a maximum value of 2 due to the spin degrees of freedom. At $U/t=10$, n_k is plotted along the diagonal $k_x=k_y=k$ in Fig. 15. At zero doping, the quasiparticle

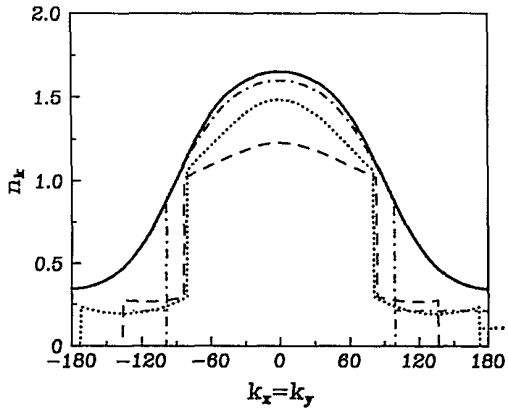

FIG. 15. Momentum distribution n_k for $k=k_x=k_y$ at $U/t=10$. Z_k vanishes for $\delta=0$ (solid line), is finite for the spirals $\delta=0.2$, 0.3 (dotted and dashed), and increases slightly for the zone state $\delta=0.4$ (dot-dashed).

weight Z_k vanishes as it must for an antiferromagnetic insulator. Away from zero doping, Z_k always has a finite value, increasing at first and then decreasing until the spiral-zone transition as displayed in Fig. 16. Increasing U/t lowers Z_k similar to the lowering in $\rho(\varepsilon_F)$ and $\hbar\omega_p$. For the ferromagnet at mean field, $Z_k=1$ just as in the noninteracting Fermi-liquid case. Column states have the highest values of $Z_k>1$. The distribution n_k includes only the mean-field correlations and it is important to determine if the fluctuation effects reduce Z_k to the values necessary to reconcile the peak widths seen in photoemission.[41]

IV. FLUCTUATIONS

Terms beyond the saddle point in the loop expansion concisely describe the fluctuations around the mean-field

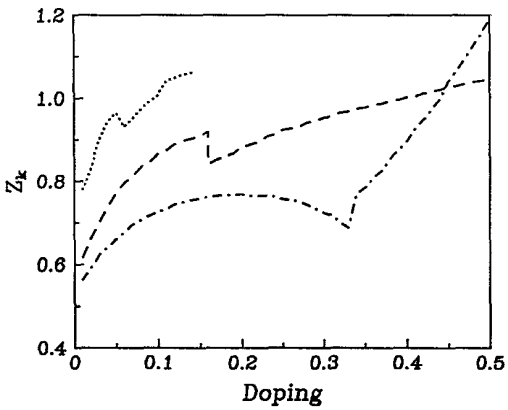

FIG. 16. Quasiparticle weight Z_k at the mean-field level decreases for increasing U/t with a discontinuity at the spiral-zone transition. $U/t=2.5$, 5, 10 is plotted as dotted, dashed, and dot-dashed, respectively. Zone states have the highest weight at the mean-field level.

twisted states. The partition function up to quadratic terms in the fluctuations $\hat{M}$ can be expressed as

$$Z=(1/\mathcal{N})\exp(-\beta\Omega_{\rm MF})\int D[\rho,\phi^a]\exp(-S_{\rm eff}) ,$$

$$\beta\Omega_{\rm MF}=\beta UL(\bar{\rho}^2+S^2)-{\rm Tr}\ln(\bar{K}) , \tag{16}$$

$$S_{\rm eff}=(\beta LU/2)[{\rm Tr}(\hat{M}^\dagger\hat{M})+(U/L\beta){\rm Tr}(\bar{K}^{-1}\hat{D}\bar{K}^{-1}\hat{D})] .$$

The second term is the $n=2$ term in the loop expansion, therefore of order $1/S^2$. At zero doping, the 36 possible electron polarization bubbles in $S_{\rm eff}$ are evaluated at $\mathbf{Q}_0$. Expressed in terms of a new order-parameter field

$$\xi^\mu=(\rho_{q,n},\phi^x_{Q_0+q,n},\phi^y_{Q_0+q,n},\phi^z_{Q_0+q,n}) ,$$

we can write $S_{\rm eff}=\beta UL\,\xi^\dagger_\mu\Gamma^{\mu\nu}\xi_\nu$ with the symmetric matrix Γ given by

$$\Gamma^{\rho\rho}_{q,n}=1+(U/\beta L)\sum_{p,m}[\Delta^{-1}_{p,m}\Delta^{-1}_{p+q,m+n}+(US)^2]G_{p,m}G_{p+q,m+n} , \tag{17a}$$

$$\Gamma^{xx}_{q,n}=1+(U/\beta L)\sum_{p,m}[\Delta^{-1}_{p+Q_0,m}\Delta^{-1}_{p+q,m+n}+(US)^2]G_{p,m}G_{p+q,m+n} , \tag{17b}$$

$$\Gamma^{x\rho}_{q,n}=-(2U/\beta L)\sum_{p,m}US\Delta^{-1}_{p,m}G_{p,m}G_{p+q,m+n} , \tag{17c}$$

$$\Gamma^{yy}_{q,n}=1+(U/\beta L)\sum_{p,m}[\Delta^{-1}_{p+Q_0,m}\Delta^{-1}_{p+q,m+n}-(US)^2]G_{p,m}G_{p+q,m+n} , \tag{17d}$$

where $\Gamma^{zz}=\Gamma^{yy}$ and $\Gamma^{y\rho}=0$. In matrix form, we can express $\Gamma=I-\Pi$, where $\Gamma^{\mu\nu}_{pq,nm}\equiv\Gamma^{\mu\nu}_{p-q,n-m}$ and I is the identity matrix $\delta^{\mu\nu}\delta_{pq}\delta_{nm}$. Integrating over the fluctuations gives $\det(\Gamma)^{-1/2}$, which shifts the thermodynamic potential

$$\Omega=\Omega_{\rm MF}+(1/2\beta){\rm Tr}\ln(I-\Pi) .$$

Expanding this trace as before results in $\sum_m{\rm Tr}(\Pi^m)/m$, which is the Gell-Mann–Bruekner RPA correction to the thermodynamic potential.[42] For large S, since $\Pi\sim 1/S^2$, the ring approximation to the Hartree-Fock thermodynamic potential converges like $1/S^{2m}$. The quadratic term also allows us to examine the stability of the saddle-point result.

In the Landau-Ginzburg action for the fluctuations of the undoped antiferromagnet, the transverse ϕ^y,ϕ^z modes are entirely decoupled while the spin amplitude and charge modes are coupled nontrivially. Stability of the saddle point imposes the constraint $\det(\Gamma^{\mu\nu}_{q,n=0})\geq 0$ on the mass-matrix for the fluctuations. At $q=0$, we find

$$\Gamma^{yy}_{0,0}=1+U(\beta L)^{-1}\sum_{p,m}G_{p,m}=0$$

by virtue of the saddle-point condition [Eq. (10)] identifying the $\phi^y_{Q_0},\phi^z_{Q_0}$ modes as the Goldstone modes. Expanding $\Gamma^{yy}_{q,n}$ around $q=n=0$ and using $\varepsilon_{k+Q_0}=-\varepsilon_k$, we find a linear dispersion $w_n^2=c^2\mathbf{q}\cdot\mathbf{q}$ consistent with the dispersion for transverse spin waves of the nonlinear σ

model. The spin-wave velocity in the long-wavelength limit can be expressed as $\hbar c/a_0=\sqrt{B/A}$ with

$$A=(U/2)\int d^2k(f_k^- - f_k^+)/(E_k^+ - E_k^-)^3 , \quad (18a)$$

$$B=(U/2)\int d^2k(f_k^- - f_k^+)/(E_k^+ E_k^-)^3 \times[2g_k - e_k^2 - 12g_k\varepsilon_k^2/(E_k^+ - E_k^-)^2] , \quad (18b)$$

where $g_k=\sin^2k_x+\sin^2k_y$ and the integrals to be evaluated over the entire Brillouin zone. Here, the derivatives of the Fermi functions have been omitted since the DOS at the Fermi level for exact half-filling vanishes. In physical units, we obtain the bare (scale-dependent) spin-velocity $\hbar c/a_0=2$ eV at $U/t=5$, which is roughly eight times larger than the experimental value[43] reflecting the significant renormalization corrections in the continuum model.[44] While these modes effectively capture the dispersion of the true spin waves in the long-wavelength limit, the complete dispersion of the physical collective modes at any $\mathbf{q}$ requires an evaluation of the transverse susceptibility[19,45] using just the polarization bubbles Π. The action for the transverse fluctuations

$$\Gamma^{yy}_{q,n}=(Aw_n^2+B\mathbf{q}\cdot\mathbf{q})/2$$

maps to the nonlinear σ model if we add the constraint $\phi^a(x)\phi^a(x)=S^2$. The coupling constant[44] of the resulting nonlinear σ model is $g=1/B$ from which we obtain the spin stiffness $\rho=UB\equiv J_{\rm eff}/2\pi$. For large U/t, $B\sim t^2/U^2$, making the spin-exchange constant $J_{\rm eff}\sim t^2/U$ exactly as in the map to the $t-J$ model. Doping-induced frustration should lead to a disordering of the σ model by increasing the effective renormalized coupling constant g. To explore this, we solve the gap equation at the fixed point $\mathbf{Q}=\mathbf{Q}_0$ away from half-filling. The renormalized g is the bare microscopic g evaluated from the coefficient B but with a doping-independent multiplicative renormalization factor Z such that[44] $g\to Zg$ gives a reasonable fit to the experimentally observed spin-wave velocities at $\delta=0$. This requires that the renormalized $g=0.675$ at half-filling. In Fig. 17, we plot an approximate renormalized g as a function of doping for $U/t=2.5$. The resulting phenomenologically renormalized g is roughly doping independent at low doping, rises for $\delta>0.05$, and disorders, i.e., $g\geq 1$ at $\delta\geq 0.09$. This is slightly lower than the full mean-field magnetic-to-paramagnetic transition which occurs at $\delta_{c3}\sim 0.14$. Therefore, we confirm that doping disorders the system even in the above approximation where only interband contributions to B have been included. A more detailed picture will energe by including derivatives of the Fermi function that arise from intraband transitions in the lower MH band when $\delta\neq 0$.

Unlike the Goldstone modes, the matrix element $\Gamma^{x\rho}_{q,n}$ mixes the charge-transfer modes $\rho_{q,n}$ with the spin-amplitude mode $\phi^x_{Q_0+q,n}$ for general $(\mathbf{q},w_n)$. However, when $w_n=0$, the mixing term $\Gamma^{\rho x}_{q,n}$ after translating $iw_m\to iw_m+\mu\equiv z_m$ gives a manifestly odd sum

$$\sum_{p,m} z_m/[z_m^2-(E_p^-)^2][z_m^2-(E_{p+q}^-)^2]=0 .$$

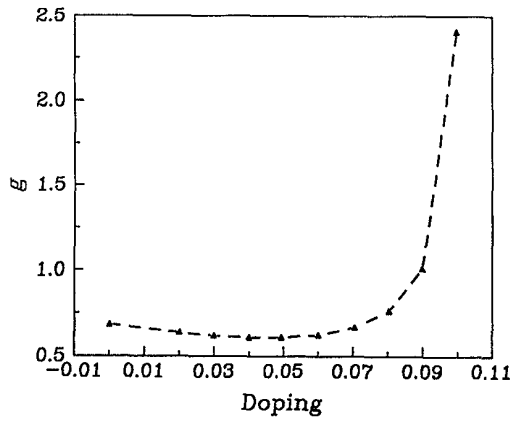

FIG. 17. The coupling constant of the nonlinear σ model increases for doping $\delta>0.05$. The coupling constant at half-filling is normalized (Ref. 39) to $g=0.685$.

Therefore, the spin-amplitude mode ϕ^x and the charge-transfer mode ρ are decoupled at zero frequency for any $\mathbf{q}$. At $q=0$, the spin-amplitude fluctuation $\phi^x_{Q_0}$ has a mass gap

$$M_-=U\Gamma^{xx}_{0,0}=U[1-12(t/U)^2+O(1/U^3)] ,$$

making use of the gap equation for S. The uniform charge fluctuation ρ_0 has mass gap $M_+=U\Gamma^{\rho\rho}_{0,0}=U$ for any U/t. Near the nesting vector $q=Q_0$, the mass gap for the ferrimagnetic spin-amplitude mode $\phi^x_{0,0}$ is M_+, while the charge-transfer mode $\rho_{Q_0,0}$ has mass M_- which approaches U, the MH gap at large U/t. The mass matrix $\Gamma^{\mu\nu}_{q,0}$ being positive definite at these two extreme points in the Brillouin zone thus establishes the stability of the saddle-point solution to long-wavelength charge-density and charge-transfer fluctuations. In light of the nonvanishing off-diagonal response function $\chi^{\rho x}$, the physical collective modes must consist of linear combinations of the spin-amplitude plus charge-fluctuation modes. At zero doping, the system exhibits insulating behavior at the one-loop level much the same as the saddle point since only interband transitions appear in the poles of the frequency sums. Away from half-filling, intraband transitions within the lower MH band will give rise to additional contributions to $M_\pm$ which will make the commensurate SDW instable. Importantly, however, for the commensurate SDW, the massless spin waves are not coupled at this order to the longitudinal spin and charge fluctuations.

The complete loss of translation invariance associated with the commensurate-incommensurate SDW transitions spells a dramatic difference for the fluctuations around the saddle point. Evaluating the polarization diagrams in the incommensurate SDW state and defining $\phi_{q,n}=\phi^x_{q,n}-i\phi^y_{q,n}$, we have the same quadratic action

$$S_{\rm eff}=\beta UL\xi^\dagger_\mu\Gamma^{\mu\nu}\xi_\nu ,$$

but with

$$\xi^{\mu}=(\rho_{q,n},\phi^{z}_{q,n}\phi_{Q+q,n},\phi^{\dagger}_{Q-q,n}) .$$

The symmetric matrix $\Gamma^{\mu\nu}$ is given by

$$\Gamma^{22}_{q,n}=1+(U/\beta L)\sum_{p,m}[\Delta^{-1}_{p,m}\Delta^{-1}_{p+q,m+n} -(US)^2]G_{p,m}G_{p+q,m+n} , \quad (19a)$$

$$2\Gamma^{33}_{q,n}=1+(U/\beta L)\sum_{p,m}\Delta^{-1}_{p+Q,m}\Delta^{-1}_{p+q,m+n}G_{p,m}G_{p+q,m+n} , \quad (19b)$$

$$2\Gamma^{34}_{q,n}=(U/\beta L)\sum_{p,m}(US)^2G_{p,m}G_{p+q,m+n} , \quad (19c)$$

$$2\Gamma^{13}_{q,n}=-(U/\beta L)\sum_{p,m}(\Delta^{-1}_{p+q,m+n}+\Delta^{-1}_{p+Q,m}) \times(USG_{p,m}G_{p+q,m+n}) , \quad (19d)$$

$$2\Gamma^{23}_{q,n}=-(U/\beta L)\sum_{p,m}(\Delta^{-1}_{p+q,m+n}-\Delta^{-1}_{p+Q,m}) \times(USG_{p,m}G_{p+q,m+n}) , \quad (19e)$$

with $\Gamma^{11}=\Gamma^{\rho\rho}$, $\Gamma^{12}=0$, $\Gamma^{14}_{q,n}=\Gamma^{13}_{-q,n}$, and $\Gamma^{24}_{q,n}$ and $-\Gamma^{23}_{-q,n}$. Since the chemical potential is now within the lower band, there are arbitrarily low-energy intraband single-particle excitations that contribute to each matrix element. However, for the incommensurate SDW, we will concentrate on the low-energy collective excitations associated with the SO(3) symmetry breaking. Classical configurations including ferromagnetism, antiferromanetism, and column states are characterized by one single axis for the local magnetic moments. Consequently, twists about the two spin axes perpendicular to this local manetization axis rotates the ground state to other states of equal energy. These broken symmetries therefore give rise to two Goldstone modes. In contrast, for a **Q** corresponding to spiral or zone states, twists about any three orthogonal spin axes lead to new configurations without altering the planar nature of these states. Alternatively, these three degrees of freedom correspond to the three Euler angles that are necessary to completely specify planar magnetic configurations. This enlarged degeneracy of the ground state implies that three massless spin-wave excitations appear in the collective fluctuation spectrum. The appearance of the third Goldstone mode at incommensurate **Q** is well known in frustrated spin models[46] and in the collective mode spectrum of continuum-field theories with nontrivial ground states like solitons and merons.[47] To see how these modes arise in the Hubbard model for incommensurate SDW solutions, we examine the effective action at the special points $\mathbf{q}=0$ and $\pm\mathbf{Q}$. At $q=0$, we find, as in the commensurate case, that $\Gamma^{13}=\Gamma^{23}=0$ resulting in the mixing of the lower two componenets ξ^3,ξ^4 only. Diagonalizing the action with respect to these two components, the mode $\phi_{Q+q}+\phi^{\dagger}_{Q=q}$ has a nonvanishing mass gap given by

$$M_{-}=(U^2S/\pi)^2\int d^2k(f^{-}_{k}-f^{+}_{k})/(E^{+}_{k}-E^{-}_{k})^3 ,$$

where we have omitted the intraband pieces proportional to derivatives of the Fermi function. In this approximation, M_{-} decreases by up to 30% from its value at half-filling at a doping near the MH band closure for $U/t=5$. Meanwhile, the mode $\phi_{Q+q}-\phi^{\dagger}_{Q-q}$ has zero mass when we make use of the saddle-point condition. This mode corresponds to rotations of the local magnetic moment around the z axis in spin space. We note that, in the limiting cases of ground states with magnetization along a single direction, the modes $\phi_{Q+q}\pm\phi^{\dagger}_{Q-q}$ become ϕ^{x}_{Q} and ϕ^{y}_{Q}, respectively, as they must. At $q=\pm Q$, we find instead that $\Gamma^{23}=\Gamma^{24}=0$, therefore decoupling the ϕ^{z} component from all the other components. Again making use of the saddle-point condition, the action becomes $\Gamma^{22}_{q=\pm Q,0}=0$ making both modes $\phi^{z}_{\pm Q}$ massless. These modes correspond to rotations of the magnetic moments out of the $x-y$ plane through twists along the x axis and the y axis in spin space. For the case of antiferromagnetism, ferromagnetism, or column states, these two modes at $\pm\mathbf{Q}$ reduce to a single mode ϕ^{z}_{Q} consistent with our calculation for the commensurate SDW. The Goldstone theorem protects the three massless modes for twisted SDW states against mass corrections in the presence of higher-loop effects. Although the massless spectrum consists of three modes as in Heisenberg models, additional massless modes corresponding to redistributions of bond exchange energies[46] will not arise for the Hubbard model since H_{MF} is, by definition, sensitive to the orientation of every local magnetic moment ϕ^{a}_{i}.

Unlike the antiferromagnet at half-filling where all charge fluctuations are decoupled from spin-wave modes to quadratic order, the twisted SDW solution couples them in a fundamental way through the terms $\Gamma^{13}_{q,n}$ and $\Gamma^{14}_{q,n}$. The nonvanshing mixing at finite momentum and frequency implies that the true eigenmodes are linear combinations of the ξ^{μ}'s. A natural consequence of this coupling on the spin-wave dispersions will be a softening of the in-plane and out-of-plane spin-wave velocities in agreement with the reduction of $\hbar c$ reported in neutron-scattering data.[43] This off-diagonal spin-charge response is a significant departure from the physical picture of noninteracting quasiparticles obtained at the saddle point. For example, in the doped antiferromagnet, the intraband charge response to an external electromagnetic field necessarily produces an accompanying magnetic twist mode. The lifetime of single-particle electronic excitations is therefore strongly influenced by scattering rates involving spin-wave exchange. This suggests a possible microscopic origin of the breakdown of conventional Fermi-liquid behavior in the normal metallic state of the copper-oxide superconductor.

V. SUMMARY

In summary, we have presented a framework from which both conventional and unconventional aspects of the normal-state properties of the copper-oxide superconductors may be understood. This has been obtained by considering fluctuation corrections to both the insulating and metallic SDW ground states of the one-band Hubbard model. Our approach allows a description of the magnetic ordering observed at very low doping. If the

double peaks seen in neutron scattering[43] in superconducting samples can be attributed to incommensurate SDW ordering, then $q \sim 0.27-0.43$ at $\delta \sim 0.11$. In our saddle-point approximation, this implies that $U/t \sim 3-4$ in close agreement with the choice based upon the on-site magnetization at half-filling. In addition, the observed reduction in the on-site magnetization with doping is also qualitatively consistent with the reduction of S obtained at the mean-field level for the twisted SDW states. Asymmetric scattering cross sections with polarized neutrons and optical dichromism as in other rare-earth spiral magnets offers a unique way to test whether single **Q** twist states are realized in the layered cuprates.[35] Any local-parity violation effects observed here would be consistent with a single **Q** twist state. However, even this signal could disappear with the doping-induced onset of short-range magnetic order which, in our framework, can be accounted for as arising from domain walls which separate regions of degenerate **Q** in otherwise homogenous samples. Spin-wave dynamics for the incommensurate SDW states is significantly altered in the presence of an additional Goldstone mode as in known rare-earth helimagnets.[46] An alternative possibility is that doping-induced reduction of the on-site magnetization may also induce pitch fluctuations and lead to a spin nematic with short-range magnetic ordering.[46]

On the electronic side, there is experimental evidence for an unconventional version of the traditional Fermi surface of a normal metal. The twist states predict a highly anisotropic Fermi surface especially at low doping. Most photoemission studies are confined to a single quadrant in the Brillouin zone and the results are not in contradiction with the twist states.[48] In the presence of domains, however, even a significantly anisotropic Fermi surface would be less distinguishable. The unconventional nature of the Fermi liquid is associated with anomalously short quasiparticle lifetimes. A more detailed study of one-loop response functions is needed to determine whether the calculated charge-spin coupling in the twisted magnetic background is responsible for the observed marginal Fermi-liquid behavior.

Finally, a doping-induced closure of the interband Mott-Hubbard charge gap occurs for every U/t. The associated rearrangement of states considerably reduces the DOS at the Fermi surface relative to the $U=0$ metal. The crossing induces a pileup of states above the Fermi surface and has a width comparable to the doping-induced peaks seen in infrared absorption.[27] The rapid lowering of the upper MH band should also be discernable in tunneling, photoemission spectroscopy (PES), and inverse PES experiments performed at various dopings. The observed sharp drop in the Hall coefficient at $\delta=0.17$ is also consistent with the drastic change in the Fermi surface. Although the upper MH band does not cross the chemical potential and change the topology of the Fermi surface, its proximity to the Fermi surface will alter scattering rates and transport coefficients even at the mean-field level. Since the mean-field electronic and magnetic properties qualitatively approximate many features of the layered perovskites, it is very suggestive that the charge-spin collective effects evident at one-loop order and perhaps higher-order scattering processes may provide explanations to the anomalous non-Fermi-liquid behavior of these systems. A careful evaluation of response functions including these effects is therefore very important.

ACKNOWLEDGMENTS

This work was supported in part by the Natural Sciences and Engineering Research Council of Canada. We gratefully acknowledge stimulating discussions with P. Coleman, A. Ruckenstein, H. Schulz, Z. Tešanović, and W. Macready. P.V. would like to thank International Centre for Theoretical Physics (ICTP) for its hospitatity where some of this work was completed.

[1]N. F. Mott, Proc. Phys. Soc. London, Sect. A **62**, 416 (1949); Rev. Mod. Phys. **40**, 677 (1968).
[2]J. G. Bednorz and K. A. Müller, Z. Phys. B **64**, 189 (1986).
[3]P. W. Anderson, Science **235**, 1196 (1987).
[4]J. Hubbard, Proc. R. Soc. London, Ser. A **276**, 238 (1963).
[5]H. R. Krishnamurthy *et al.*, Phys. Rev. Lett. **64**, 950 (1990); C. L. Kane *et al.*, Phys. Rev. B **41**, 2653 (1990); B. I. Shraiman and E. D. Siggia, Phys. Rev. Lett. **62**, 1564 (1989); C. Jayaprakash, H. R. Krishnamurty, and S. Sarkar, Phys. Rev. B **40**, 2610 (1989).
[6]P. W. Anderson *et al.*, Phys. Rev. Lett. **58**, 2790 (1988).
[7]I. Affleck and B. J. Marston, Phys. Rev. B **37**, 3774 (1988).
[8]X. G. Wen, F. Wilczek, and A. Zee, Phys. Rev. B **39**, 11 413 (1989).
[9]See references in Dung-Hai Lee and Charles L. Kane, Phys. Rev. Lett. **64**, 1313 (1990).
[10]P. W. Anderson, Int. J. Mod. Phys. B **4**, 181 (1990); C. M. Varma *et al.*, Phys. Rev. Lett. **63**, 1996 (1989).
[11]See, for example, S. Doniach and E. H. Sondheimer, *Green's Functions for Solid State Physicists* (Bengamin, Reading, 1974), p. 184.
[12]P. V. thanks Zlatko Tešanović and H. Schulz for pointing this out.
[13]P. W. Anderson, Phys. Rev. D **86**, 694 (1952).
[14]See, for example, G. W. Semenoff and L. C. R. Wijewardhana (unpublished).
[15]J. A. Vergés, E. Louis, P. S. Lomdahl, F. Guinea, and A. R. Bishop (unpublished).
[16]See, for example, A. Fetter and J. D. Walecka, *Quantum Theory of Many Particle Systems* (McGraw-Hill, New York, 1971), p. 247.
[17]A. Moreo *et al.*, Phys. Rev B **41**, 2313 (1990).
[18]R. J. Birgeneau *et al.*, Phys. Rev. B **38**, 6614 (1988); **39**, 2868 (1989); J. M. Tranquada *et al.*, *ibid.* **38**, 2477 (1988).
[19]J. R. Schrieffer, X-G. Wen, and S. C. Zhang, Phys. Rev. B **39**, 11 663 (1989); A. Singh and Z. Tešanović, *ibid.* **41**, 614 (1990).
[20]M. Takahashi, J. Phys. C **10**, 1289 (1977).
[21]Y. Tokura *et al.*, Physica C **162-164**, 1231 (1989).

[22]B. I. Shraiman and Eric D. Siggia, Phys. Rev. B **40**, 9162 (1989).
[23]H. J. Schulz (unpublished).
[24]H. J. Schulz, Phys. Rev. Lett. **64**, 1445 (1990).
[25]J. E. Hirsch, Phys. Rev. B **31**, 4403 (1985).
[26]A. Weidinger *et al.*, Phys. Rev. Lett. **62**, 102 (1989).
[27]T. Takahashi *et al.*, Nature **334**, 691 (1988): Y. Sakisaka *et al.*, Phys. Rev. B **39**, 2304 (1989); S. Etemad *et al.*, *ibid.* **37**, 3396 (1988).
[28]Y. Sakisaka *et al.*, Phys. Rev. B **42**, 4189 (1990).
[29]N. P. Ong *et al.*, Phys. Rev. B **35**, 8807 (1987); H. Takagi, S. Uchida, and Y. Tokura, Phys. Rev. Lett. **62**, 1197 (1989).
[30]H. J. Schulz, J. Phys. (Paris) **50**, 2833 (1989).
[31]L. Lilly *et al.*, Phys. Rev. Lett. **65**, 1379 (1990).
[32]L. B. Ioffe and A. I. Larkin, Phys. Rev. B **37**, 5730 (1988); M. Marder *et al.*, *ibid.* **41**, 6920 (1990).
[33]V. J. Emery, S. A. Kivelson, and H. Q. Lin, Phys. Rev. Lett. **64**, 475 (1990).
[34]J. D. Jorgensen *et al.*, Phys. Rev. B **38**, 11 337 (1988).
[35]A. W. Overhauser, Phys. Rev. **128**, 1437 (1962).
[36]E. Fenton and Hanyou Chu (unpublished).
[37]P. B. Allen, W. E. Pickett, and H. Krakauer, Phys. Rev. B **37**, 7482 (1988).
[38]S. Tajima *et al.*, *Proceedings of the Second International Symposium on Superconductivity, Tsukuba, Japan* (Springer-Verlag, Berlin, 1990).
[39]See references in M. Grilli *et al.*, Phys. Rev. B **42**, 329 (1990); **37**, 7482 (1988).
[40]D. Pines, *The Many-Body Problem* (Benjamin/Cummings, Reading, 1961), p. 34.
[41]C. G. Olson *et al.*, Science **245**, 731 (1989).
[42]J. W. Negele and H. Orland, *Quantum Many-Particle Systems* (Addison-Wesley, Reading, 1988), p. 332.
[43]G. Shirane *et al.*, Phys. Rev. Lett. **59**, 1613 (1987); G. Aeppli *et al.*, *ibid.* **62**, 2052 (1989); K. Yamada *et al.*, Phys. Rev. B **40**, 4557 (1989); D. Vaknin *et al.*, Phys. Rev. Lett. **58**, 2802 (1987).
[44]S. Chakraverty, *High Temperature Superconductivity* (Addison-Wesley, Reading, 1989), p. 136.
[45]G. Vignale and M. R. Hedayati, Phys. Rev. B **42**, 786 (1990).
[46]See references in P. Chandra, P. Coleman, and A. I. Larkin (unpublished).
[47]A. Jevicki, Nucl. Phys. B **127**, 125 (1977).
[48]J. C. Campuzano *et al.*, Phys. Rev. Lett. **64**, 2308 (1990).